Journal Pre-proofs

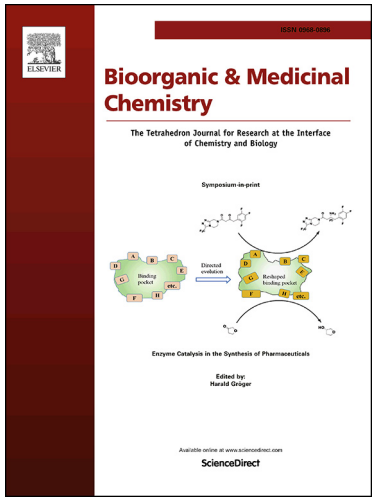

Synthesis and highly potent anti-inflammatory activity of licofelone- and ketorolac-based 1-arylpyrrolizin-3-ones

Damian A. Madrigal, Carlos H. Escalante, Gabriel A. Gutiérrez-Rebolledo, José M. Cristobal-Luna, Omar Gómez-García, Roberto I. Hernández-Benitez, Ana L. Esquivel-Campos, Salud Pérez-Gutiérrez, Germán A. Chamorro-Cevallos, Francisco Delgado, Joaquín Tamariz

PII: S0968-0896(19)30503-6
DOI: https://doi.org/10.1016/j.bmc.2019.115053
Reference: BMC 115053

To appear in: *Bioorganic & Medicinal Chemistry*

Received Date: 28 March 2019
Revised Date: 18 August 2019
Accepted Date: 19 August 2019

Please cite this article as: Madrigal, D.A., Escalante, C.H., Gutiérrez-Rebolledo, G.A., Cristobal-Luna, J.M., Gómez-García, O., Hernández-Benitez, R.I., Esquivel-Campos, A.L., Pérez-Gutiérrez, S., Chamorro-Cevallos, G.A., Delgado, F., Tamariz, J., Synthesis and highly potent anti-inflammatory activity of licofelone- and ketorolac-based 1-arylpyrrolizin-3-ones, *Bioorganic & Medicinal Chemistry* (2019), doi: https://doi.org/10.1016/j.bmc.2019.115053

Synthesis and highly potent anti-inflammatory activity of licofelone- and ketorolac-based 1-arylpyrrolizin-3-ones

Damian A. Madrigal,[a,b,†] Carlos H. Escalante,[a,†] Gabriel A. Gutiérrez-Rebolledo,[b] José M. Cristobal-Luna,[b] Omar Gómez-García,[a] Roberto I. Hernández-Benítez,[a] Ana L. Esquivel-Campos,[c] Salud Pérez-Gutiérrez,[c] Germán A. Chamorro-Cevallos,[b,*] Francisco Delgado[a] and Joaquín Tamariz[a,*]

[a] *Departamento de Química Orgánica, Escuela Nacional de Ciencias Biológicas, Instituto Politécnico Nacional. Prol. Carpio y Plan de Ayala S/N, 11340 Mexico City, Mexico;* [b] *Departamento de Farmacia, Escuela Nacional de Ciencias Biológicas, Instituto Politécnico Nacional. Av. Wilfrido Massieu S/N, Unidad Adolfo López Mateos, 07738 Mexico City, Mexico;* [c] *Departamento de Sistemas Biológicos, Universidad Autónoma Metropolitana, Unidad Xochimilco. Calzada del Hueso 1100, Col. Villa Quietud, 04960 Mexico City, Mexico*

* Corresponding authors. Tel.: +52 55 57296300/52398 (G.A.C.-C.), +52 55 57296300/62411 (J.T.)

E-mail addresses: gchamcev@yahoo.com.mx (G.A.C.-C.), jtamarizm@gmail.com (J.T.)

† The authors contributed equally to this work.

Abstract— Since NSAIDs are commonly used anti-inflammatory agents that produce adverse effects, there have been ongoing efforts to develop more effective and less toxic compounds. Based on the structure of the anti-inflammatory pyrrolizines licofelone and ketorolac, a series of 1-arylpyrrolizin-3-ones was synthesized. Also prepared was a series of substituted pyrroles, mimicking similar known anti-inflammatory agents. The anti-inflammatory activity of the test compounds was determined with a phorbol ester (TPA)-induced murine ear edema protocol. For the most active derivatives, **19b-c**/**20b-c**, the anti-inflammatory effect was the same as that of the reference compound (indomethacin) and was dose-dependent. These compounds have an aryl ring at the C-1 position and a methoxycarbonyl group at the C-2 position of the pyrrolizine framework, which represent plausible pharmacophore groups with anti-inflammatory activity. The anti-inflammatory activity of 1-substituted analogs containing a five- or six-membered heterocycles was lower but still good, while that of the pyrroles was only moderate. Although the docking studies suggests that the effect of analogs **19a–c**/**20a–c** is associated with the inhibition of cyclooxygenase-2, experimental assays did not corroborate this idea. Indeed, a significant inhibition of NO was found experimentally as a plausible mechanism of action.

Keywords: 1-Arylpyrrolizin-3-ones, Substituted pyrroles, Anti-inflammatory activity, Licofelone, Ketorolac, TPA induced ear edema model.

1. Introduction

The inflammatory process is an immune response to a perturbation of the homeostatic equilibrium of the organism, whether endogenous (e.g., genetic and ageing) or exogenous (e.g., injury and nutrition).[1-3] In addition to providing a defense against challenges to homeostasis, this process is involved in many acute and chronic diseases such as arthritis, cancer and diabetes,[4,5] as well as cardiovascular[6,7] and neurodegenerative disorders.[8] Hence, the medications often prescribed for such diseases are steroidal anti-inflammatory agents.[9]

The non-steroidal anti-inflammatory drugs (NSAIDs) with a mechanism of action related to the non-selective inhibition of cyclooxygenase-1 (COX-1), COX-2 and 5-lipoxygenase (5-LOX) produce serious adverse effects, including peptic ulcers,[10–12] renal failure[13] and cardiovascular diseases.[14] Consequently, there have been ongoing efforts during many years to seek effective alternatives with less toxicity.

COX-1, COX-2 and 5-LOX are among the key enzymes involved in the transformation of leukotrienes to prostaglandins, the latter of which are key inflammatory mediators.[15] Indeed, most NSAIDs, including pyrrolizidines,[16] were designed to target and inhibit these enzymes. Licofelone (**1**)[17–19] and the clinically used ketorolac (**2a**)[20] are pyrrolizine-based NSAIDs that act as potent selective and nonselective inhibitors of COX-1/COX-2/5-LOX[21] and COX-1/COX-2 enzymes, respectively (Figure 1).

Its mechanism of action of ketorolac (**2a**), classified as an NSAIDs with potent analgesic and moderate anti-inflammatory effects,[22,23] is the inhibition of the prostaglandin synthesis through unspecific inactivation of both COX isoforms (1 and 2). This drug is used clinically to relieve acute pain associated with inflammation. In research, it is usually employed as a reference drug for murine models of analgesia rather than acute inflammation.[24] Its pharmacological mechanism is similar to that exhibited by indomethacin,[25] which mainly serves as a reference drug in murine models of acute inflammation.[26–28]

An abundance of pyrrolizine-based compounds has been synthesized recently for evaluation as potential anti-inflammatory agents. Many are highly active derivatives and selective COX-1/COX-2/5-LOX inhibitors, such as compounds **1**,[29] **2b**[20] and **3-5**,[30–33] (Figure 1) among other analogs.[16,33,34]

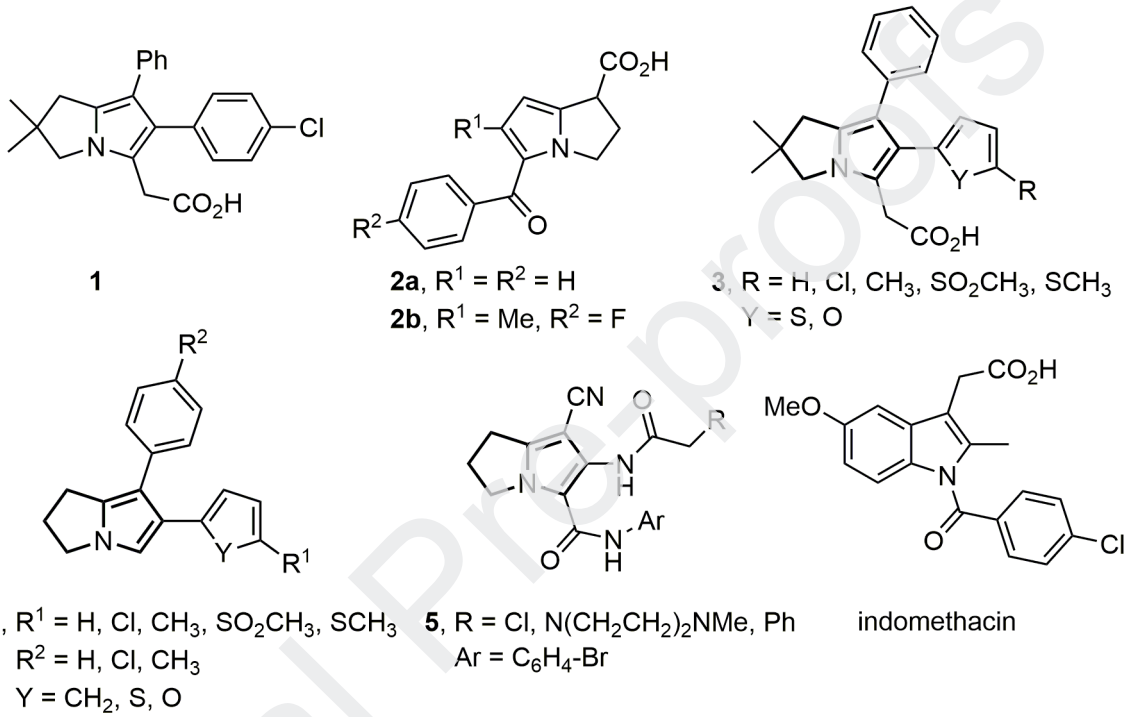

Figure 1. Licofelone (**1**), ketorolac (**2a**), indomethacin and anti-inflammatory pyrrolizine-based analogs **2b** and **3-5**.

Pyrrole-based anti-inflammatory agents have also been designed,[35–38] such as the potent derivatives **6a-b**[39] and **6c-d**[40] as well as NSAIDs tolmetin (**7a**) and zomepirac (**7b**) (Figure 2).[41]

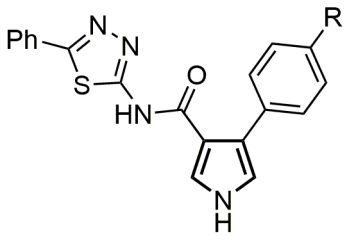

6a, R = NO_2
6b, R = F

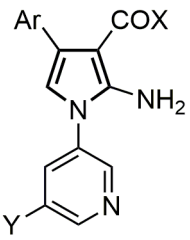

6c, X = OEt, Ar = C_6H_4-4-Cl
6d, X = NH_2, Ar = C_6H_4-4-Cl
Y = H, CF_3

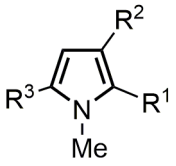

7a, R^1 = CH_2CO_2H, R^2 = H, R^3 = COC_6H_4-4-Me
7b, R^1 = COC_6H_4-4-Cl, R^2 = Me, R^3 = CH_2CO_2Na

Figure 2. Anti-inflammatory pyrrole-based analogs **6a-d** and **7a-b**.

The aim of the current contribution was to synthesize a series of pyrroles **10-15** and pyrrolizines **19a-g**/**20a-g** in order to assess their anti-inflammatory effect on the formation of ear edema induced by 12-*O*-tetradecanoylphorbol-13-acetate (TPA) in male CD1 mice.[42] This anti-inflammatory protocol was chosen because it is a reliable model for testing potential anti-inflammatory agents capable of inhibiting the arachidonic acid biosynthetic pathway and in this way hampering the formation of prostaglandins, which in turn inhibits the activity of COX and 5-LOX enzymes.[43–45]

2. Results and discussion

2.1. Chemistry

Pyrrole-containing agents were presently designed based on the potent anti-inflammatory activity found with certain *N*-methyl 5-aroylpyrrole-2-acetic acids.[46] Accordingly, a formyl group was introduced at the C-2 position of the pyrrole ring and the acetic acid equivalent at the nitrogen atom. Since 2-formylpyrrole (**8a**) can serve as a

building block for the divergent synthesis of substituted pyrroles[47] and pyrrolizines,[48] it was herein adopted for the preparation of these simple pyrrole derivatives. Hence, the preparation of the series of substituted pyrroles **10**, **11**, and **13**–**15** was achieved by the readily efficient functionalization of **8a** (Scheme 1). The alkylation of **8a** with methyl bromoacetate (**9**) under basic conditions provided **10** in almost quantitative yield. By thermal treatment of **10** with *N,N*-dimethylformamide dimethyl acetal (DMFDMA), enaminone **11** was obtained in good yield as a single *Z* isomer (Scheme 1).

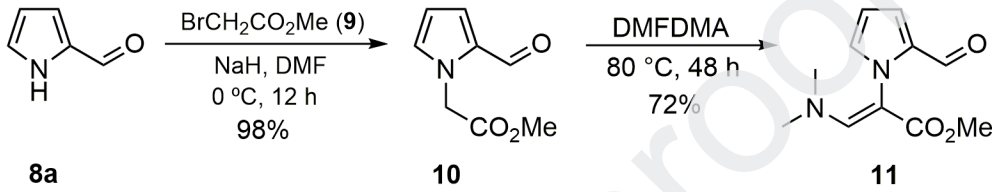

Scheme 1. Preparation of 2-formylpyrrole analogs **10** and **11**.

The Knoevenagel reaction of **10** with methylene-activated compound **12a** under acid conditions,[49] through an organocatalytic condensation carried out by acetic acid ammonium salts,[50] gave the expected condensation product **13** as a single *E* stereoisomer (Scheme 2). However, under the usual bromination conditions with NBS, pyrrole **13** was converted into an inseparable mixture *E*/*Z* of diastereoisomers **14**/**15** (81:19). Despite this unexpected result, the latter brominated analogs were prepared due to the important anti-inflammatory activity found for synthetic and natural bromopyrroles,[51,52] and the increased lipid solubility of the brominated derivatives of some NSAIDs, which reduce inflammation better than bromine-free agents.[53]

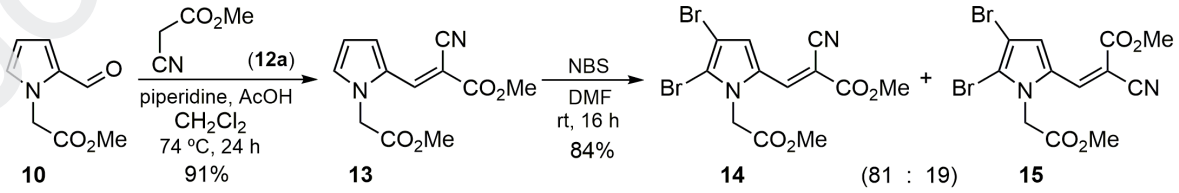

Scheme 2. Preparation of the mixture of pyrrole analogs **14**/**15**.

The synthetic approach for the preparation of 1-arylpyrrolizidin-3-ones **19a-g** was envisioned based on a previously reported strategy.[54] The series of Knoevenagel derivatives **17a-g** was prepared by the condensation of aldehydes **16a-g** with dimethyl malonate (**12b**) under catalysis with piperidine/AcOH.[49] The conjugate addition of pyrrole (**8b**) to derivatives **17a-g** was carried out with iodine or aluminum chloride as the catalyst, leading to the corresponding adducts **18a-g** in moderate to good yields (Table 1).

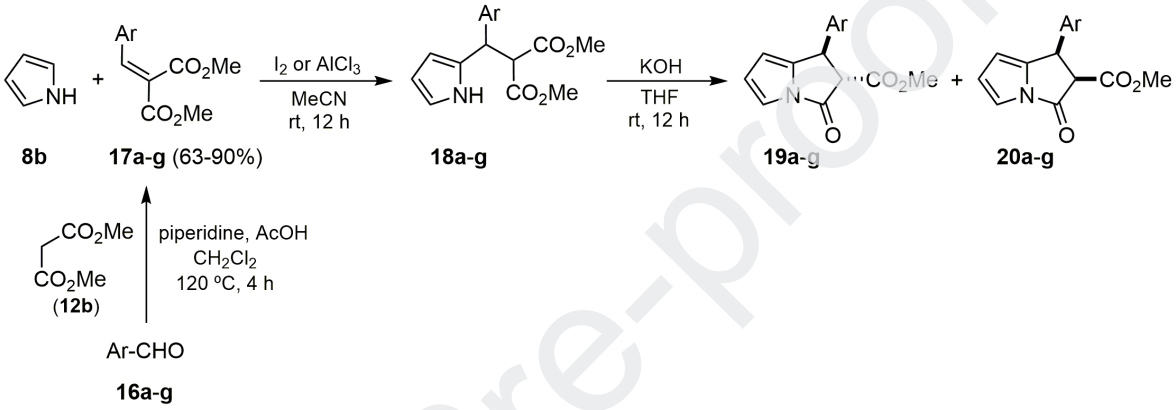

Scheme 3. Preparation of 1-arylpyrrolizidin-3-ones **19a-g**/**20a-g**.

The last step of the cyclization of adducts **18a-g** to 1-substituted pyrrolizin-3-ones **19a-g** was achieved by employing previously described conditions, with sodium hydride as the base.[54] Most adducts **18a-g** were different from those already reported but resulted in low yields prompting the exploration of other bases. For example, after reacting the substrate with KOH in anhydrous THF and stirring at room temperature for 12 h, the desired pyrrolizin-3-ones were obtained in moderate to good yields as inseparable mixtures of *anti/syn* diastereoisomers **19a-g**/**20a-g** (Table 2). The *anti* pyrrolizin-3-ones **19a-g** were afforded as the main isomers in high diastereoisomeric ratio (*dr*).[55] The structure of each product was established by ^{1}H and ^{13}C NMR assisted by 1D and 2D experiments (NOE, HMQC and HMBC) and HRMS.

Table 1. Reaction conditions, ratios and yields for the preparation of **18a-g** and the mixtures **19a-g**/**20a-g**.[a]

Entry	**17** (Ar)	Lewis acid	**18** (%)[b]	**19**/**20** (ratio)[c] (%)[b]
1	**17a** (C_6H_4-4-NO_2)	I_2	**18a** (78)	**19a**/**20a** (91:9)(78)
2	**17b** (C_6H_4-4-CN)	I_2	**18b** (77)	**19b**/**20b** (92:8)(66)
3	**17c** (C_6H_4-4-Br)	I_2	**18c** (29)	**19c**/**20c** (90:10)(57)
4	**17d** (C_6H_4-3-OMe)	I_2	**18d** (49)	**19d**/**20d** (90:10)(57)
5	**17e** (furan-2-yl)	$AlCl_3$	**18e** (24)	**19e**/**20e** (92:8)(80)
6	**17f** (thiophen-2-yl)	I_2	**18f** (53)	**19f**/**20f** (93:7)(66)
7	**17g** (pyridin-2-yl)	$AlCl_3$	**18g** (64)	**19g**/**20g** (93:7)(70)

[a] For the preparation of **18a-g**, the reactions were carried out with **17** (1.0 mol equiv), **8b** (3.0 mol equiv) and I_2 or $AlCl_3$ (0.5 mol equiv) in anh. MeCN at rt for 12 h. For the preparation of **19a-g**/**20a-g**, the reactions involved **18** (1.0 mol equiv) and KOH (1.1 mol equiv) in anh. THF at rt for 12 h.
[b] Determined by ^{1}H NMR.
[c] After purification by column chromatography.

Owing to the difficulty of separating the **19**/**20** mixtures by flash column chromatography and HPLC, base-promoted C-2 epimerization was used to isomerize the minor isomer to the major one (thermodynamic isomer). Instead of the epimerization, however, the aromatization of the A ring took place in modest to good yields. Thus, the **19a**/**20a** (91:9) mixture was treated with NaOMe to afford the novel pyrrolizine **21a** in 42% yield (Scheme 4). The yield was slightly improved by treating **19a**/**20a** (91:9) with DDQ as the oxidant. A better yield of pyrrolizine **21b** was obtained by the reaction of **19c**/**20c** (90:10) with DDQ.

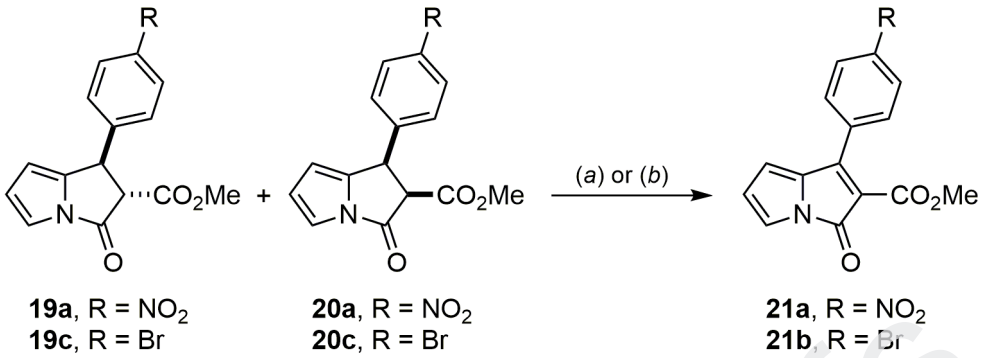

Scheme 4. Preparation of pyrrolizines **21a** and **21b**. *Reaction conditions:* (*a*) MeONa/MeOH (1.0 M) (2.0 mol equiv.), THF, 50 °C, 2 h, **21a** (42%). (*b*) DDQ (2.0 mol equiv.), CH_2Cl_2, rt, 12 h; **21a** (46%), **21b** (70%).

2.2. Anti-inflammatory activity

A single dose (2 mg/ear) of each test compound or indomethacin was applied to a TPA-induced edema on the mouse ear. Compared to the control animals (subjected to a TPA-induced edema but not given any anti-inflammatory treatment), there was significant inhibitory activity generated by functionalized pyrroles **10**, **11** and **14**/**15** (81:19), with values of 33.73%, 21.37%, and 15.63%, respectively (Table 2). Interestingly, the structurally simplest compound (**10**) was the most active, although none of these compounds were comparable to indomethacin (41.47%). Hence, an assay involving lower doses was not contemplated. Indomethacin herein served as the positive control because of being more effective than other drugs (e.g., nimesulide or ketorolac) for reducing TPA-induced inflammation.[56,57] Additionally, it is known that the mechanism of action of indomethacin is the inhibition of COX-1/COX-2,[25] and the interaction between indomethacin and COX-2 has been corroborated by docking.

The anti-inflammatory effect of the series of pyrrolizines **19**/**20** was evaluated as well. The decision to use the mixture of epimers was supported by the docking studies, which revealed that both had similar interaction energy with the enzymes (vide infra). Thus, each inseparable mixture of the pyrrolizine series was administered in a single dose of 2 mg/ear, producing a significant decrease in the development of edema ($p < 0.05$; *vs.* the control

animals with an untreated TPA-induced edema). Contrary to the functionalized pyrroles, all the measured effects of the series of pyrrolizines were equivalent to those of the reference drug (indomethacin). In particular, two mixtures of the pyrrolizines, **19b**/**20b** and **19c**/**20c**, afforded inhibition of inflammation equivalent to that elicited by the reference drug.

Table 2. Anti-inflammatory activity of pyrrole derivatives **10**, **11** and **14**/**15** (81:19) on a TPA-induced ear edema in male CD1 mice [a]

Treatment	Ear edema formation (mg)	Percentage of inhibition (%)
TPA control	17.91±1.20	---
indomethacin	10.49±0.62[b]	41.47
10	11.87±0.40[bc]	33.73
11	14.09±0.45[bc]	21.37
14/**15** (81:19)	15.11±0.87[bc]	15.63

[a] Data are expressed as the mean ± standard error of the mean (SEM) (n = 7). All compounds were administered at the dose of 2 mg/ear. The percentage of inhibition of the edema was calculated in relation to the TPA control group (considered as 100%), in which a TPA-induced edema was not treated by any anti-inflammatory agent. Results were processed with two-way analysis of variance (ANOVA) and the post-hoc Student-Newman-Keuls test ($p < 0.05$).
[b] *vs.* TPA control.
[c] *vs.* indomethacin.

As a consequence of the positive results with the pyrrolizines, each element of the series was tested at three doses to evaluate its anti-inflammatory effect on the formation of the ear edema induced by TPA in male CD1 mice (Table 3). Due to the dose-dependent response found for all pyrrolizine compounds, the equation representing the inhibitory effect *vs.* dose could be ascertained. The median effective dose (ED_{50}) values were calculated for each derivative during diverse phases of acute inflammation, thus establishing initial doses for future experiments in murine models related to chronic inflammation.[58] Whereas the 1.38 mg/ear determined for derivatives **19c**/**20c** and **19b**/**20b** is similar to the 1.29 mg/ear for indomethacin, the 1.54 mg/ear for **19a**/**20a** was significantly different than the reference drug. Nevertheless, the latter mixture exerted a good anti-inflammatory effect with a single topical application at 2 mg/ear (Table 3).

Compared to **19a-c**/**20a-c**, a lower inhibitory activity was shown by derivatives **19e**/**20e** (2.75 mg/ear) and **19g**/**20g** (3.63 mg/ear), which contain a heterocycle at the C-1

position. Although the latter two mixtures exhibited significantly lower anti-inflammatory activity, the result of a single topically-applied dose of 2 mg/ear was noticeable compared to the control group (Table 3). Derivatives **19d**/**20d** and **19f**/**20f** proved to be moderately active anti-inflammatory agents. Since all compounds were administered topically, lipophilicity probably played a key role in the observed effects, which may explain why the aryl-substituted pyrrolizines produced greater inhibition than the C-1 heterocyclic-substituted analogs.

Table 3. Percentage of inhibition and median effective doses (ED_{50}) of derivatives **19**/**20** and **21** on the TPA-induced ear edema in male CD1 mice.[a]

Treatment	Doses (mg/ear)	Ear edema formation (mg)	Percentage of inhibition (%)	ED_{50} (mg/ear)
TPA control	-	17.61 ± 1.06	---	---
indomethacin	0.5	11.22 ± 0.35[b]	32.12	1.29 (R^2 = 0.99)
	1	9.01 ± 0.25•[b]	45.49	
	2	6.99 ± 0.13•*[b]	57.68	
19c/**20c** (90:10)	0.5	11.17 ± 0.40[b]	32.39	1.38 (R^2 = 0.98)
	1	9.59 ± 0.21•[b]	41.97	
	2	7.17 ± 0.24•*[b]	56.61	
19b/**20b** (92:8)	0.5	11.12 ± 0.24[b]	32.74	1.38 (R^2 = 0.96)
	1	9.43 ± 0.17•[b]	42.94	
	2	7.23 ± 0.18•*[b]	56.27	
19a/**20a** (91:9)	0.5	11.18 ± 0.59[b]	32.40	1.54 (R^2 = 0.97)
	1	9.62 ± 0.35•[b]	41.77	
	2	7.77 ± 0.11•*[bc]	52.95	
19e/**20e** (92:8)	0.5	15.19 ± 0.47[bc]	13.73	2.75 (R^2 = 0.95)
	1	12.77 ± 0.66•[bc]	27.40	
	2	9.25 ± 0.50•*[bc]	47.45	
19d/**20d** (90:10)	0.5	16.74 ± 0.27[c]	4.93	3.02 (R^2 = 0.92)
	1	13.46 ± 0.45•[bc]	23.52	
	2	9.69 ± 0.37•*[bc]	44.97	
19g/**20g** (93:7)	0.5	16.68 ± 0.10[c]	5.25	3.63 (R^2 = 0.88)
	1	14.49 ± 0.35•[bc]	17.70	
	2	9.79 ± 0.26•*[bc]	44.35	
19f/**20f** (93:7)	0.5	15.19 ± 0.30[bc]	13.70	3.89 (R^2 = 0.92)
	1	13.80 ± 0.44•[bc]	21.61	
	2	10.02 ± 0.53•*[bc]	43.09	

[a] Data are expressed as the mean ± SEM for each group (n=7). The percentage of inhibition of the edema was calculated as a percentage of the value of inflammation determined for the control group (considered as 100%), in which a TPA-induced edema was not treated by any anti-inflammatory agent. Results were processed with two-way analysis of variance (ANOVA) and post-hoc Student-Newman-Keuls test ($p < 0.05$). • *vs*. 0.5 mg/ear; * *vs*. 1 mg/ear.
[b] *vs*. TPA control.
[c] *vs.* indomethacin.

Novel pyrrolizines **21a** and **21b** were also evaluated as potential anti-inflammatory agents. Following the aforementioned method of TPA-induced ear edema in male CD1 mice, both compounds were tested at three doses, exerting a dose-dependent effect very similar to that produced by indomethacin (Table 4). Although **21a** was less active (ED_{50} = 1.86 mg/ear) than indomethacin (ED_{50} = 1.07 mg/ear), it exhibited a greater percentage of inhibition than **21b** (ED_{50} = 3.23 mg/ear). It is worth noticing that this pattern is contrary to taht found with the same C-1 aryl substituents in the series of mixtures **19**/**20**, where **19c**/**20c** was more active than **19a**/**20a**.

Table 4. Percentage of inhibition generated by derivatives **21a** and **21b** on the TPA-induced ear edema in male CD1 mice, and the corresponding median effective doses (ED_{50}).[a]

Treatment	Doses (mg/ear)	Ear edema formation (mg)	Percentage of inhibition (%)	ED_{50} (mg/ear)
TPA control	-	19.82 ± 0.69	---	---
Indomethacin	0.5	11.51 ± 0.27[b]	41.94	1.07 (R^2 = 0.99)
	1	9.44 ± 0.12[•b]	52.37	
	2	7.71 ± 0.22[•*b]	61.10	
21a	0.5	18.13 ± 0.26[bc]	8.52	1.86 (R^2 = 0.95)
	1	15.04 ± 0.47[•bc]	24.10	
	2	9.23 ± 0.32[•*bc]	53.43	
21b	0.5	18.14 ± 0.24[bc]	8.46	3.23 (R^2 = 0.95)
	1	13.93 ± 0.70[•bc]	29.73	
	2	11.72 ± 0.59[•*bcd]	40.88	

[a] Data are expressed as the mean ± SEM for each group (n=7). The percentage of inhibition of the edema was calculated as a percentage of the value of inflammation determined for the control group (considered as 100%), in which a TPA-induced edema was not treated by any anti-inflammatory agent. Results were processed with two-way analysis of variance (ANOVA) and post-hoc Student-Newman-Keuls test ($p < 0.05$). • *vs*. 0.5 mg/ear; * *vs*. 1 mg/ear.
[b] *vs*. TPA control.
[c] *vs*. indomethacin.
[d] *vs*. compound **21a**.

Regarding the epimeric compounds **19**/**20** and considering the difference of the TPA control values, **21a** showed a higher ED_{50} value (1.86 mg/ear) than **19a**/**20a** (1.54 mg/ear), but lower than **19e**/**20e** (2.75 mg/ear). Interestingly, the ED_{50} value was lower for **21b** (3.23 mg/ear) than for the mixtures **19f**/**20f** and **19g**/**20g**, indicating the greater activity of the former.

Independently of the role played by the C-1 and C-2 substituents, the current results suggest that the C-1 and C-2 stereocenters of pyrrolizin-3-ones **19a-g**/**20a-g** do not represent an exclusive factor for the promotion of anti-inflammatory activity, but are indeed an essential element in improving such an effect. Consequently, both *anti* (**19a-g**) and *syn* (**20a-g**) stereoisomers are probably responsible for inhibiting inflammation (Table 3).

Since indomethacin and the series of pyrrolizines **19**/**20** demonstrated a comparable anti-inflammatory effect, they may have the same mode of action involving the inhibition of COX-1/COX-2.[29] Likewise, the epimeric pyrrolizine series shares similar structural features with licofelone (**1**) and ketorolac (**2a**). Therefore, their mechanism of action is likely to be analogous, meaning that the reduction found in the ear edema could be due to the inhibition of prostaglandin synthesis by targeting either COX-1/COX-2 or COX-2/5-LOX.[21,29,32,33]

*2.3. Docking of the analogs **19a-g**/**20a-g** with the COX-2 enzyme*

Molecular docking of pyrrolizin-3-ones **19a-g**/**20a-g** was carried out at the active site of the COX-2 enzyme (Tables 5 and S1) on the AutoDock/AutoDockTools program, [59] based on the crystal structure of this enzyme retrieved from the Protein Data Bank.[60] The docking results for indomethacin are included as a reference. Derivatives **19a-c**, having electron-withdrawing groups (NO_2, CN and Br) in *para* position of the aromatic ring, showed a better binding energy than **19d** (bearing an electron-donor group in the aromatic ring) and **19e-g** (with heteroaromatic rings). The binding energy of **19a** was the closest to that of indomethacin. A similar trend was observed in the binding energy of the *syn*-epimers **20a-g**, finding better values for **20a-c** (-8.07 to -8.82 kcal/mol) than **20d-g** (-6.07 to -7.16 kcal/mol).

The binding mode and the protein-ligand interactions of **19a-g**/**20a-g** are depicted in Figures 3 and S1. When the binding mode of indomethacin was analyzed at the active site of the COX-2 enzyme, most of the residues involved in the interaction coincided with those previously reported from docking studies on this enzyme.[61–63] The binding mode of the

most active compound, **19a**, shares certain key hydrophilic interactions with the reference drug indomethacin. For example, a conventional hydrogen bond and a carbon hydrogen bond were formed between the NO_2 group of **19a** (equivalent to the carboxylic acid moiety of indomethacin) and the side chain of Arg120 and Tyr355. Moreover, both the phenyl ring of indomethacin and the pyrrole ring of **19a** displayed π-alkyl interactions with Val523. The same π-alkyl interaction takes place for almost the entire *anti* series, while in the *syn* series it is seen with the C-1 aryl ring or the C-1 heterocyclic ring. The most active compound of the *syn*-series, **20a**, exhibits π-alkyl type interactions with Val523 and Ala527, as occurs with indomethacin.

Most interactions between the test compounds and the amino acids of the active site of the enzyme were hydrophobic. However, hydrophilic interactions were identified between most pyrrolizine derivatives and the amino acids Tyr385, Tyr355 and Arg120. In the series of *anti*-derivatives **19a-g**, there were π-alkyl type interactions between the C-1 aryl ring with Val349 and Leu531. These *anti*-derivatives also showed π-alkyl interactions with Leu352 and Ala527, as occurred with the *syn*-derivatives, involving the C-1 aryl ring in the series **19a-d** and the heterocyclic ring in **19e-g**. Additionally, a π-sigma interaction existed between the Val523 amino acid and the C-1 aryl or heterocyclic ring of all *syn*-derivatives **20a-g**.

The binding orientation of the *anti*-compounds (Figures 4 and S2) is illustrated by the overlay of five of the analogs, **19a-d** and **19g** (Figure 4A), showing their similarity with each other and with indomethacin (Figure 4B). Thus, a comparable binding region is observed for the pyrrolizine framework and the C-2 methoxycarbonyl group of the derivatives and the *N*-(4-chlorobenzoyl) group of indomethacin (Figure 4B). It is noteworthy that the polar substituents of the C-1 aryl ring of **19a-d** have similar protein-ligand contacts as the C-3 carboxylic acid of indomethacin (see the interactions with amino acids Arg120 and/or Tyr355, Figures 3 and S1), which was not the case for the heterocycles of **19e-g** (Figure 4C).

These polar interactions may play a significant role not only in creating the differences in the interaction energies, but also in the *in vivo* anti-inflammatory effects. A correlation was found between the biological activity and molecular docking results of derivatives **19a-**

c, which have aryl polar substituents. This series of derivatives was the most active, producing an inhibition of 52.95-56.61%, very close to the value for indomethacin (57.68%). The compounds containing heterocyclic rings, on the other hand, elicited an inhibition of 43.09-47.45%.

The *anti*-series **19a-g** and the *syn*-series **20a-d** and **20g** had distinct binding orientations. For the latter series, the C-1 aryl ring occupies the same position as the benzo moiety of the indole frame of indomethacin (Figure 4D), and the aryl polar substituents are oriented in the same position as the methoxy group of indomethacin (Figure S2). Hence, these substituents probably provide an important contribution to the interaction energy of the ligand with the protein.

Table 5. Docking results of indomethacin and pyrrolizines **19a-c**, **19e** and **20a** at the active site of COX-2.

Compound	Binding energy ΔG (kcal/mol)	Interacting Residues	Polar Interactions	Hydrophobic Interactions
indomethacin	-9.76	His90, Val116, Arg120, Val349, Leu352, Ser353, Tyr355, Leu384, Tyr385, Trp387, Arg513, Phe518, Met522, Val523, Gly526, Ala527, Ser530, Leu531.	Arg120 C-H…..O Arg120 N-H…..O Tyr355 O-H…..O Ser530 C-H…..O	π-alkyl (Leu352, Trp387, Val523, Ala527). π-sigma (Val349). alkyl (Val349, Leu384, Met522, Ala 527, Leu531).
19a	-9.34	Arg120, Val344, Ty348, Val349, Leu352, Tyr355, Phe381, Leu384, Tyr385, Trp387, Phe518, Met522, Val523, Gly526, Ala527, Ser530, Leu531.	Arg120 C-H…..O Arg120 N-H…..O Tyr355 O-H…..O Tyr385 O-H…..O	π-alkyl (Val349, Met522, Val523). π-sigma (Ala527). π-π T-shaped (Trp387).
19b	-8.62	Arg120, Val344, Tyr348, Val349, Leu352, Phe381, Tyr385, Met522, Val523, Gly526, Ala527, Ser530, Leu531.	Arg120 N-H…..N Tyr385 O-H…..O	π-alkyl (Leu531, Leu352, Val523). π-sigma (Val349, Ala527). amide π-stacked (Gly526).
19c	-7.95	Arg120, Val344, Tyr348, Val349, Leu352, Phe381, Tyr385, Met522, Val523, Gly526, Ala527, Ser530, Leu531.	Tyr385 O-H…..O	π-alkyl (Leu531, Val523). π-sigma (Val349, Ala527). alkyl (Leu531).

19e	-6.52	Tyr348, Val349, Leu352, Tyr355, Phe381, Leu384, Trp387, Met522, Val523, Gly526, Ala527, Ser530.	Tyr385 O-H…..O	π-alkyl (Val349, Met522, Val523). π-sigma (Ala527). π–π T-shaped (Trp387).
20a	-8.82	His90, Tyr348, Val349, Leu352, Ser353, Tyr355, Phe381, Leu384, Tyr385, Trp387, Arg513, Phe518, Met522, Val523, Gly526, Ala527, Ser530.	Tyr385 O-H…..O	π-alkyl (Leu352, Ala527). π-sigma (Val523). amide π-stacked (Gly526).

Indomethacin

19a

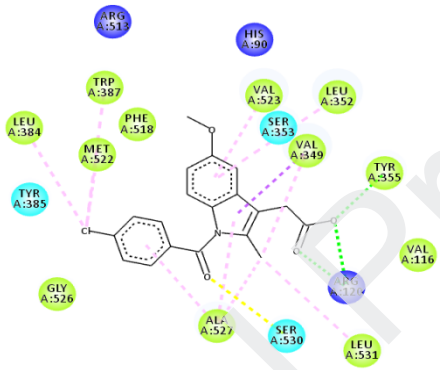

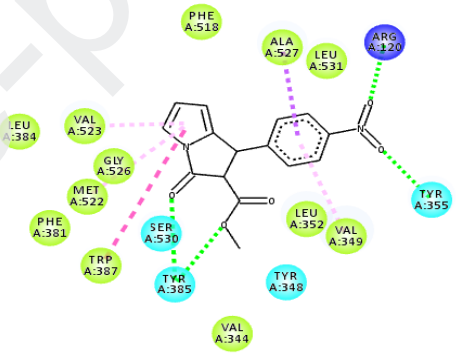

19b

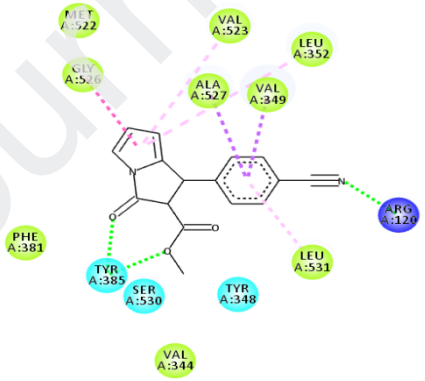

19c

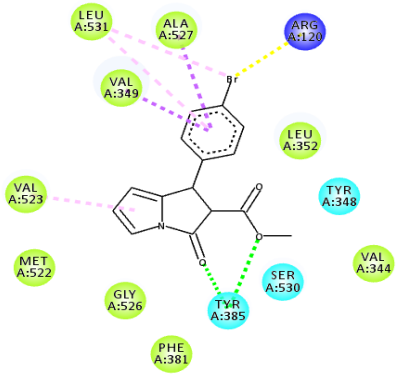

19e

20a

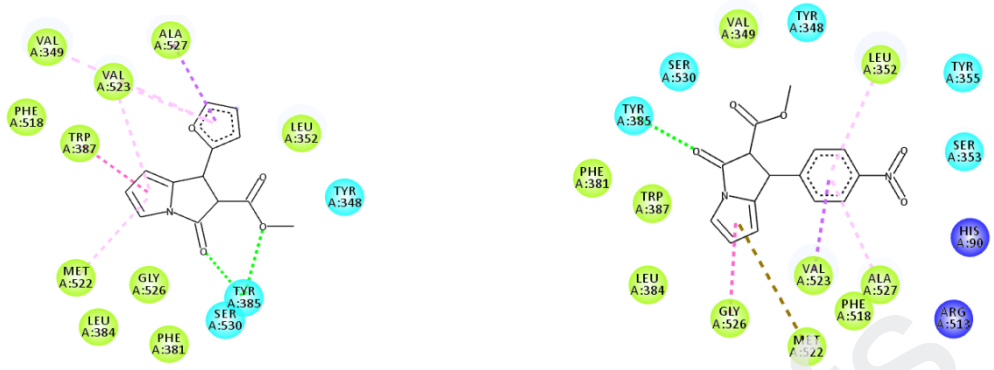

Figure 3. The predicted binding mode of indomethacin and pyrrolizines **19a-c**, **19e** and **20a** at the active site of the COX-2 enzyme. The 2D model shows the amino acids involved in such binding. The following interactions are portrayed with dotted lines: conventional hydrogen bonds (green), carbon-hydrogen (yellow), π-sigma (purple), π-alkyl (light pink), amide-π stacking (dark pink) and π–π T-shaped (orange). The basic amino acids are denoted in blue, hydrophobic in green and polar in cyan.

A

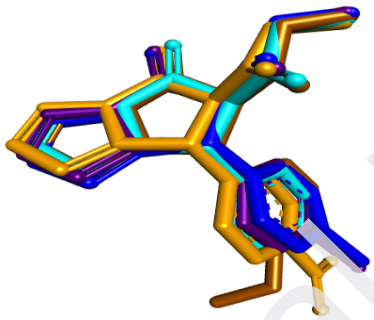

B

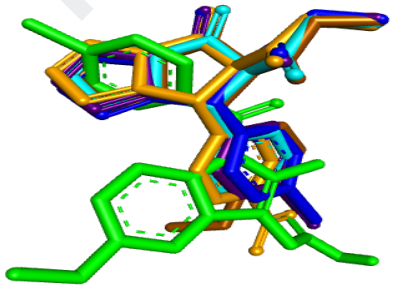

C

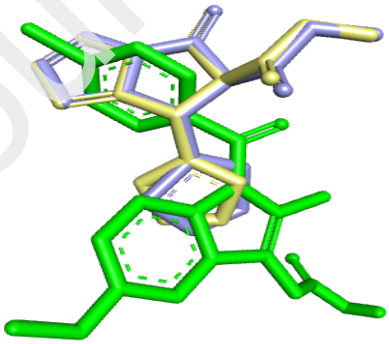

D

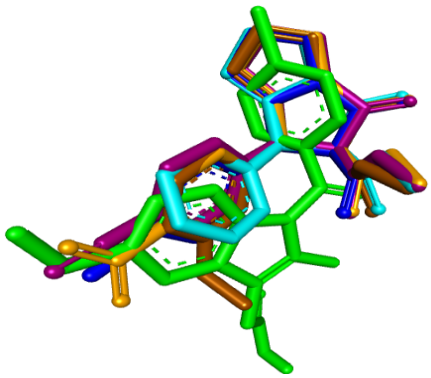

Figure 4. A. Overlay of the docking poses of **19a** (orange), **19b** (purple), **19c** (dark blue), **19d** (brown) and **19g** (cyan). B. Comparison of the binding mode of each of the respective groups of compounds **19a-d** and **19g** to that of indomethacin (green). C. Overlay of **19e** (light green) and **19f** (light blue). D. Overlay of **20a** (orange), **20b** (purple), **20c** (dark blue), **20d** (brown) and **20g** (cyan), and comparison of the binding mode of each of the corresponding groups of compounds **20a-d** and **20g** to that of indomethacin (green).

*2.4. COX-2 enzyme and nitric oxide inhibitory activity of **19a-c/20a-c***

According to the docking study, the inhibitory effect on COX-2 produced by the series of pyrrolizin-3-ones **19a-g**/**20a-g** represents a possible mechanism of action for their strong anti-inflammatory activity on the TPA-induced ear edema. Hence, *in vitro* COX-2 inhibition assays were explored in relation to these *in silico* findings. In the cell viability tests,[64] the J774A.1 macrophages (8×10^4 cells/well) were treated with the most effective mixtures of pyrrolizin-3-ones, **19a-c**/**20a-c**, at concentrations of 6.25 to 200 µg/mL dissolved in DMSO. Only the mixture **19b**/**20b** showed no toxicity at the concentrations evaluated (Figure S3). However, **19a**/**20a** and **19c**/**20c** displayed toxicity at concentration of 50 µg/mL. Therefore, the epimers were used at concentration of 25 µg/mL in subsequent experiments, resulting in an IC_{50} of 80.82, <200 µg/mL and 74.94 for **19a**/**20a**, **19b**/**20b** and **19c**/**20c**, respectively. The lack of effect of the three mixtures on the mRNA expression of COX-2 could be due to their inability to inhibit its production at this concentration. Moreover, the apparent contradiction between the *in vivo* inhibition of COX-2 and *in vitro* cytotoxicity has been previously observed for an anti-inflammatory drug and potential anticancer agent (celecoxib), which is explained by the fact that the effect caused in each model occurs is by independent mechanism of action.[65]

Lipolisacharide (LPS), a component of the membrane of gram-negative bacteria, promotes the generation of pro-inflammatory cytokines and nitric oxide (NO) in macrophages.[66] NO is a signaling molecule with several effects, such as vasodilation, host defense, inflammation and blood clotting.[67] In inflammatory processes the overproduction of NO can activate nuclear factor kappa B (NF-κB) and trigger the expression of proinflammatory mediators. Arise in the levels of NO elicited by inducible nitric oxide synthase (iNOS) can lead to tissue damage.[68] Hence, the inhibition of NO production in macrophages is a potential therapeutic strategy for inflammation.

In the present study, the three mixtures **19a**/**20a**–**19c**/**20c** significantly lowered the level of NO in LPS-stimulated J774A.1 macrophages (1 x 10^6 cells/well), which was assessed by measuring the presence of nitrites through the Griess reaction.[69] Firstly, it was herein confirmed that the level of nitrites was markedly increased when the macrophages were exposed to LPS (Figure 5). The value of the nitrite concentration after LPS exposure was set at 100%, and the basal value (prior to LPS exposure) was found to be 61.19%. At 25 µg/mL, **19a**/**20a**, **19b**/**20b** and **19c**/**20c** generated a very significant inhibition of nitrites production, with values of 63.63%, 64.75% and 63.52%, respectively. These percentage nitrite levels were similar to the basal value and to the inhibition obtained with indomethacin (64.63%) at the same concentration (25 µg/mL).

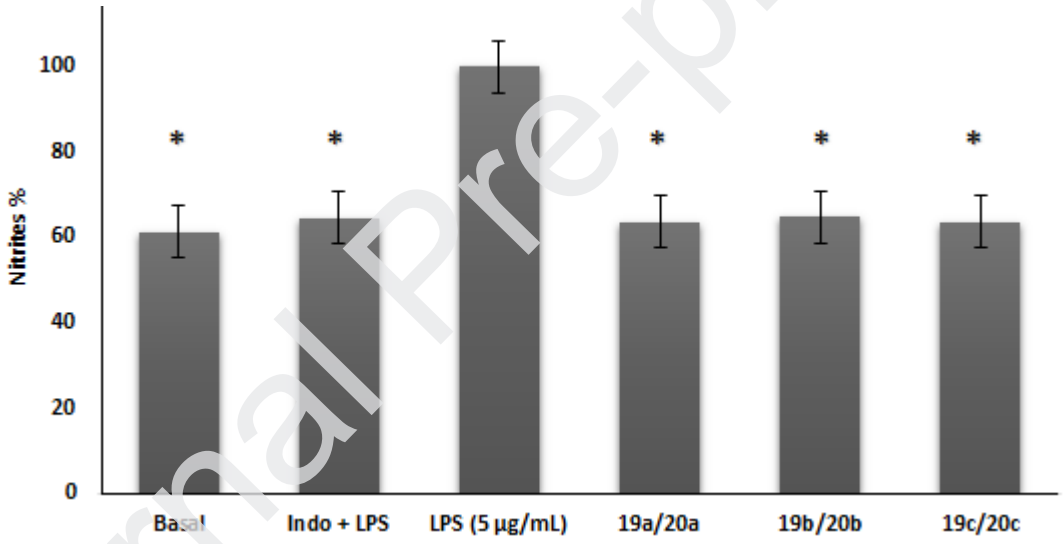

Figure 5. Effect of **19a**/**20a**, **19b**/**20b**, **19c**/**20c** and indomethacin (Indo) (at 25 µg/mL) on the level of nitrites in LPS-stimulated macrophages. The basal value was 61.19%. Data represent the mean ± SEM of three independent experiments. * $p < 0.05$ *vs.* LPS.

3. Conclusion

A series of pyrroles **10**, **11** and **14**/**15**, pyrrolizin-3-ones **19a-g**/**20a-g** and pyrrolizines **21a-b** were herein synthesized and tested, finding a moderate to high anti-inflammatory effect. The median effective doses of some **19a-g**/**20a-g** and **21a** derivatives caused over

50% inhibition of the ear edema formation. Compounds **19b-c**/**20b-c** proved to be the most active licofelone- and ketorolac-based analogs, showing an anti-inflammatory effect comparable to indomethacin. Docking studies performed on the COX-2 enzyme established multiple molecular modeling interactions between the active site and the different polar and non-polar functional groups of the derivatives. Plausible pharmacophore groups responsible for the anti-inflammatory effect of **19b-c**/**20b-c** include the C-1 functionalized aryl ring and the C-2 methoxycarbonyl group. These pyrrolizine compounds provide good structural requirements for the design of more active analogs in the future. The C-1 substituted benzene ring apparently serves a key function as the hydrophobic (benzene ring) and hydrophilic (polar substituent) moiety, possibly representing a good and versatile scaffold to promote the formation of valuable active substituents. Due in part to the activity shown by pyrrolizines **21a-b**, it appears that the C-1 and C-2 stereogenic centers are not an exclusive condition for the anti-inflammatory effect of the derivatives **19a-g**/**20a-g**, but do indeed improve such an effect.

According to the docking results, the mechanism of action for the reduction of the TPA-induced ear edema is likely to be the inhibition of COX-2. However, no experimental evidence corroborated the viability of this mechanistic pathway. On the other hand, the most active mixtures **19a**/**20a**–**19c**/**20c** exhibited a significant inhibition of NO production (i.e., a decrease in the level of nitrites) in LPS-stimulated macrophages. Whereas iNOS inhibition can be a plausible mechanism of action, the COX-2 inhibition cannot be completely ruled out.

The next step by our group in the investigation of the anti-inflammatory effect of these isomers will be their evaluation in a model of sub-plantar carrageenan-induced mouse paw edema. This of course implies having previously carried out studies of acute toxicity in mice with the two isomers orally or intraperitoneally administered.

4. **Experimental section**

4.1. Chemistry

Melting points were determined on an Electrothermal apparatus and are uncorrected. Infrared spectra (IR) were recorded on a FT-IR 2000 Perkin-Elmer spectrometer. ^{1}H (300 or 500 or 600 MHz) and ^{13}C (75.4 or 125 or 150 MHz) NMR spectra were obtained on

Varian Mercury-300 or Varian VNMR System or Bruker Avance III instruments, with TMS as internal standard and chemical shifts (δ) are reported in ppm. Mass Spectra were achieved on a Polaris Q-Trace GC Ultra (Finnigan Co.). High-resolution mass spectra (HRMS), in electron impact mode, were recorded on Jeol JSM-GCMateII. A Multi-Therm Benchmark, Model H5000-HC served as a heating and cooling shaker for enzymatic stability assays. Commercial reagents were used as received from Aldrich and anhydrous solvents were obtained by a distillation process. Thin layer chromatography was performed on precoated silica gel plates (Merck $60F_{254}$) and column chromatography with silica gel (230-400 mesh).

*4.2.1. Methyl 2-(2-formyl-1H-pyrrol-1-yl)acetate (**10**)*[70]

After a mixture of **8a** (0.300 g, 3.16 mmol) and NaH (0.148 g, 3.7 mmol) in dry DMF was stirred at 0 °C for 30 min, **9** (0.530 g, 3.4 mmol) was added and stirred at 0 °C for 12 h. Water (20 mL) was added and the mixture was extracted with hexane/EtOAc (1:1) (2 x 50 mL), the organic layer dried (Na_2SO_4) and the solvent removed under vacuum. The residue was purified by column chromatography over silica gel (20 g/g crude, hexane/EtOAc, 8:2) to afford **10** (0.516 g, 98%) as a yellow oil. R_f 0.53 (hexane/EtOAc, 8:2). IR (film): ῡ 3114, 2955, 2811, 1757, 1659, 1532, 1483, 1410, 1369, 1322, 1217, 1081, 1032, 1001, 766, 698 cm^{-1}. ^1H NMR (300 MHz, $CDCl_3$): δ 3.77 (s 3H, CO_2CH_3), 5.70 (s, 2H, CH_2), 6.31 (dd, J = 4.2, 2.7 Hz, 1H, H-4'), 6.92-6.94 (m, 1H, H-5'), 7.00 (dd, J = 4.2, 1.5 Hz, 1H, H-3'), 9.53 (d, J = 0.9 Hz, 1H, C*H*O). ^{13}C NMR (75.4 MHz, $CDCl_3$): δ 50.1 (CH_2), 52.5 (CO_2CH_3), 110.2 (C-4'), 124.6 (C-3'), 131.6 (C-2'), 132.0 (C-5'), 168.8 (CO_2CH_3), 179.8 (*C*HO). HRMS (EI): *m/z* [M+] calcd for $C_8H_9NO_3$: 167.0582; found: 167.0584.

*4.2.2. Methyl (E)-3-(Dimethylamino)-2-(2-formyl-1H-pyrrol-1-yl)acrylate (**11**)*

In a threaded ACE glass pressure tube with a sealed Teflon screw cap and magnetic stirring bar, a mixture of **10** (0.300 g, 1.8 mmol) and DMFDMA (0.66 g, 5.5 mmol) was stirred at 80 °C for 48 h. The mixture was diluted with CH_2Cl_2 (5 mL) and the solvent was removed under vacuum. The residue was purified by column chromatography over silica gel (20 g/g crude, hexane/EtOAc, 1:1) to furnish **11** (0.287 g, 72%) as a yellow oil. R_f 0.30

(hexane/EtOAc, 7:3). IR (film): ῡ 2949, 1694, 1665, 1620, 1528, 1469, 1433, 1390, 1367, 1308, 1215, 1107, 1079 cm^{-1}. ^1H NMR (500 MHz, $CDCl_3$): δ 2.67 (br s, 6H, $N(CH_3)_2$), 3.64 (s, 3H, CO_2CH_3), 6.31 (dd, *J* = 4.3, 2.5 Hz, 1H, H-4'), 6.82-6.84 (m, 1H, H-5'), 7.03 (dd, *J* = 4.3, 2.0 Hz, 1H, H-3'), 7.53 (s, 1H, H-3), 9.58 (s, 1H, CHO). ^{13}C NMR (125 MHz, $CDCl_3$): δ 51.4 (CO_2CH_3), 97.5 (C-2), 110.3 (C-4'), 121.0 (C-3'), 134.1 (C-5'), 134.8 (C-2'), 146.2 (C-3), 167.3 (CO_2CH_3), 179.7 (CHO). HRMS (EI): *m/z* [M+] calcd for: $C_{11}H_{14}N_2O_3$: 222.1005; found: 222.1005.

*4.2.3. Methyl (E)-2-Cyano-3-(1-(2-methoxy-2-oxoethyl)-1H-pyrrol-2-yl)acrylate (**13**)*

In a threaded ACE glass pressure tube with a sealed Teflon screw cap and magnetic stirring bar, a mixture of **10** (0.10 g, 0.6 mmol), **12a** (0.064 g, 0.65 mmol), piperidine (0.025 g, 0.29 mmol) and glacial AcOH (0.028 g, 0.47 mmol) in CH_2Cl_2 (5 mL) was stirred at 70 °C for 24 h. The mixture was diluted CH_2Cl_2 (50 mL) and washed with water (25 mL) and a saturated aqueous solution of $NaHCO_3$ until neutral. The organic layer was dried (Na_2SO_4) and the solvent removed under vacuum. The residue was purified by column chromatography over silica gel (20 g/g crude, hexane/EtOAc, 8:2), to give **13** (0.135 g, 91%) as a pale yellow solid. R_f 0.4 (hexane/EtOAc, 7:3); mp 125-126 °C. IR (KBr): ῡ 3113, 2963, 2213, 1741, 1711, 1592, 1477, 1450, 1435, 1413, 1355. 1269, 1201, 1090, 1009, 756, 675 cm^{-1}. ^1H NMR (300 MHz, $CDCl_3$): δ 3.80 (s, 3H, CO_2CH_3), 3.89 (s, 3H, CO_2CH_3), 4.84 (s, 2H, CH_2CO_2Me), 6.47 (ddd, *J* = 4.2, 2.6, 0.6 Hz, 1H, H-4'), 7.05 (dd, *J* = 2.6, 1.5 Hz, 1H, H-5'), 7.80 (dm, *J* = 4.2 Hz, 1H, H-3'), 7.92 (s, 1H, H-3). ^{13}C NMR (75.4 MHz, $CDCl_3$): δ 48.1 (CH_2CO_2Me), 53.0 (CO_2CH_3), 53.1 (CO_2CH_3), 94.0 (C-2), 112.8 (C-4'), 116.7 (CN), 120.3 (C-3'), 127.2 (C-2'), 131.3 (C-5'), 138.9 (C-3), 164.3 (CO_2CH_3), 167.7 (CO_2CH_3). HRMS (EI): *m/z* [M+] calcd for: $C_{12}H_{12}N_2O_4$: 248.0797; found: 248.0797.

*4.2.4. Methyl (E)-2-Cyano-3-(4,5-dibromo-1-(2-methoxy-2-oxoethyl)-1H-pyrrol-2-yl)acrylate (**14**). Methyl (Z)-2-Cyano-3-(4,5-dibromo-1-(2-methoxy-2-oxoethyl)-1H-pyrrol-2-yl)acrylate (**15**)*

A solution of NBS (0.14 g, 0.8 mmol) in dry DMF (3 mL) was added dropwise to a stirred solution of **13** (0.100 g, 0.40 mmol) in dry DMF (3 mL) at 0 °C. The mixture was stirred at room temperature for 16 h, then a mixture of hexane/EtOAc/H_2O (1:1:0.5) (30

mL) was added. The organic layer was dried (Na_2SO_4) and the solvent removed under vacuum. The residue was purified by column chromatography over silica gel (20 g/g crude, hexane/EtOAc, 7:3) to afford a mixture of **14/15** (81:19) (0.137 g, 84%) as a yellow solid. R_f 0.32 (hexane/EtOAc, 8:3); mp 279-281 °C. IR (KBr): ῡ 2956, 2217, 1749, 1721, 1586, 1438, 1407, 1384, 1259, 1219, 1095, 1043, 770 cm^{-1}. ^1H NMR (500 MHz, $CDCl_3$): δ 3.82 (s, 3H, CO_2CH_3), 3.90 (s, 3H, CO_2CH_3), 4.93 (s, 2H, $CH_2CO_2CH_3$), 7.82 (d, J = 0.5 Hz, 1H, H-3'), 7.83 (d, J = 0.5 Hz, 1H, H-3). Signals attributed to the minor isomer **15**: δ 3.80 (s, CO_2CH_3), 3.93 (s, CO_2CH_3), 4.90 (s, $CH_2CO_2CH_3$), 7.99 (s, H-3 or H-3'). ^{13}C NMR (125 MHz, $CDCl_3$): δ 47.6 ($CH_2CO_2CH_3$), 53.2 (CO_2CH_3), 53.3 (CO_2CH_3), 96.2 (C-2), 104.0 (C-4'), 116.0 (C-5'), 116.4 (CN), 121.0 (C-3'), 128.5 (C-2'), 137.5 (C-3), 163.5 (CO_2CH_3), 166.5 (CO_2CH_3). Signals attributed to the minor isomer **15**: δ 50.4, 53.6, 103.5, 107.0, 114.9, 125.6, 127.4, 138.3, 162.4, 166.4. HRMS (EI): *m/z* [M+] calcd for: $C_{12}H_{10}Br_2N_2O_4$: 403.9008; found: 403.9009.

*4.2.5. Dimethyl 2-(4-Nitrobenzylidene)malonate (**17a**)*[71]

In a threaded ACE glass pressure tube with a sealed Teflon screw cap and magnetic stirring bar, a mixture of **16a** (0.300 g, 1.99 mmol), **12b** (0.289 g, 2.19 mmol), piperidine (0.085 g, 1.00 mmol) and glacial AcOH (0.060 g, 1.00 mmol) in CH_2Cl_2 (1.0 mL) was heated to 120 °C for 4 h. The mixture was diluted with CH_2Cl_2 (40 mL) and washed with H_2O (20 mL) and a saturated aqueous solution of $NaHCO_3$ until neutral. The organic layer was dried (Na_2SO_4) and the solvent removed under vacuum. The residue was purified by column chromatography over silica gel (10 g/g crude, hexane/EtOAc, 95:5) to deliver **17a** (0.475 g, 90%) as a colorless solid. R_f 0.60 (hexane/EtOAc, 7:3); mp 135-137 °C [Lit.[71] 135-136 °C]. IR (KBr): ῡ 3112, 2959, 1727, 1631, 1601, 1517, 1435, 1346, 1258, 1225, 1199, 1062, 979, 940, 852, 765, 720, 687 cm^{-1}. ^1H NMR (500 MHz, $CDCl_3$): δ 3.84 (s, 3H, CO_2CH_3), 3.89 (s, 3H, CO_2CH_3), 7.56-7.60 (m, 2H, H-2"), 7.80 (s, 1H, H-1'), 8.22-8.26 (m, 2H, H-3"). ^{13}C NMR (125 MHz, $CDCl_3$): δ 52.9 (CO_2CH_3), 53.0 (CO_2CH_3), 124.0 (C-3"), 129.3 (C-2), 129.9 (C-2"), 139.1 (C-1"), 139.9 (C-1'), 148.5 (C-4"), 163.7 (CO_2CH_3), 166.0 (CO_2CH_3). HRMS (EI): *m/z* [M+] calcd for $C_{12}H_{11}NO_6$: 265.0586; found: 265.0580.

*4.2.6. Dimethyl 2-(4-Cyanobenzylidene)malonate (**17b**)*[71]

Following the method of preparation for **17a**, the reaction of **16b** (0.300 g, 2.29 mmol), **12a** (0.333 g, 2.52 mmol), piperidine (0.098 g, 1.15 mmol) and glacial AcOH (0.069 g, 1.15 mmol) provided **17b** (0.453 g, 81%) as a colorless solid. R_f 0.48 (hexane/EtOAc, 7:3); mp 97-98 °C [Lit.[71] 97-98 °C]. IR (KBr): ῡ 3038, 2959, 2223, 1739, 1719, 1628, 1440, 1373, 1265, 1223, 1202, 1064, 974, 934, 826 cm^{-1}. ^1H NMR (500 MHz, $CDCl_3$): δ 3.84 (s, 3H, CO_2CH_3), 3.87 (s, 3H, CO_2CH_3), 7.52 (dm, J = 8.5 Hz, 2H, H-2"), 7.68 (dm, J = 8.5 Hz, 2H, H-3"), 7.75 (s, 1H, H-1'). ^{13}C NMR (125 MHz, $CDCl_3$): δ 52.9 (CO_2CH_3), 53.0 (CO_2CH_3), 113.8 (C-4"), 118.1 (CN), 128.7 (C-2), 129.6 (C-2"), 132.5 (C-3"), 137.2 (C-1"), 140.4 (C-1'), 163.8 (CO_2CH_3), 166.1 (CO_2CH_3). HRMS (EI): *m/z* [M+] calcd for $C_{13}H_{11}NO_4$: 245.0688; found: 245.0688.

*4.2.7. Dimethyl 2-(4-Bromobenzylidene)malonate (**17c**)[71]*

Following the method of preparation for **17a**, the reaction of **16c** (0.500 g, 2.70 mmol), **12b** (0.392 g, 2.97 mmol), piperidine (0.115 g, 1.35 mmol) and glacial AcOH (0.081 g, 1.35 mmol) produced **17c** (0.580 g, 72%) as a colorless oil. R_f 0.55 (hexane/EtOAc, 8:2). IR (film): ῡ 2953, 1731, 1629, 1588, 1489, 1437, 1374, 1264, 1223, 1072, 1001, 838, 818 cm^{-1}. ^1H NMR (500 MHz, $CDCl_3$): δ 3.83 (s, 3H, CO_2CH_3), 3.84 (s, 3H, CO_2CH_3), 7.27 (dm, J = 8.5 Hz, 2H, H-2"), 7.50 (dm, J = 8.5 Hz, 2H, H-3"), 7.68 (s, 1H, H-1'). ^{13}C NMR (125 MHz, $CDCl_3$): δ 52.7 ($2CO_2CH_3$), 125.1 (C-4"), 126.1 (C-2), 130.6 (C-2"), 131.6 (C-1"), 132.1 (C-3"), 141.4 (C-1'), 164.1 (CO_2CH_3), 166.7 (CO_2CH_3). HRMS (EI): *m/z* [M+] calcd for $C_{12}H_{11}BrO_4$: 297.9841; found: 297.9848.

*4.2.8. Dimethyl 2-(3-Methoxybenzylidene)malonate (**17d**)*

Following the method of preparation for **17a**, the reaction of **16d** (0.500 g, 3.67 mmol), **12b** (0.534 g, 4.40 mmol), piperidine (0.157 g, 1.84 mmol) and glacial AcOH (0.110 g, 1.84 mmol) formed **17d** (0.579 g, 63%) as a reddish solid. R_f 0.31 (hexane/EtOAc, 8:2); mp 82-83 °C [Lit.[71] 81-82 °C]. IR (film): ῡ 2954, 1732, 1629, 1579, 1436, 1240, 1069, 785, 690 cm^{-1}. ^1H NMR (500 MHz, $CDCl_3$): δ 3.80 (s, 3H, OCH_3), 3.84 (s, 6H, $2CO_2CH_3$), 6.95 (dd, J = 7.5, 2.5 Hz, 1H, H-4"), 6.96 (br s, 1H, H-2"), 7.01 (br d, J = 7.5 Hz, 1H, H-6"), 7.29 (t, J = 7.5 Hz, 1H, H-5"), 7.74 (s, 1H, H-1'). ^{13}C NMR (125 MHz, $CDCl_3$): δ 52.66 (CO_2CH_3), 52.67 (CO_2CH_3), 55.2 (OCH_3), 114.2 (C-2"), 116.7 (C-4"), 121.9 (C-6"), 125.7 (C-2),

129.9 (C-5"), 134.0 (C-1"), 142.8 (C-1'), 159.8 (C-3"), 164.4 (CO_2CH_3), 167.1 (CO_2CH_3). HRMS (EI): *m/z* [M+] calcd for $C_{13}H_{14}O_5$: 250.0841; found: 250.0848.

*4.2.9. Dimethyl 2-(Furan-2-yl-methylene)malonate (**17e**)*

Following the method of preparation for **17a**, the reaction of **16e** (0.300 g, 3.13 mmol), **12b** (0.454 g, 3.44 mmol), piperidine (0.133 g, 1.57 mmol) and glacial AcOH (0.094 g, 1.57 mmol) resulted in **17e** (0.565 g, 86%) as an amber oil. R_f 0.50 (hexane/EtOAc, 7:3). IR (film): ῡ 3130, 2954, 1730, 1633, 1437, 1257, 1224, 1207, 1083, 1064, 1021, 756 cm^{-1}. ^1H NMR (500 MHz, $CDCl_3$): δ 3.83 (s, 3H, CO_2CH_3), 3.92 (s, 3H, CO_2CH_3), 6.50 (dd, *J* = 3.5, 2.0 Hz, 1H, H-4"), 6.77 (d, *J* = 3.5 Hz, 1H, H-3"), 7.48 (s, 1H, H-1'), 7.53 (brd, *J* = 2.0 Hz, 1H, H-5"). ^{13}C NMR (125 MHz, $CDCl_3$): δ 52.4 (CO_2CH_3), 52.5 (CO_2CH_3), 112.6 (C-4"), 118.2 (C-3"), 121.2 (C-2), 128.1 (C-1'), 146.3 (C-5"), 148.8 (C-2"), 164.5 (CO_2CH_3), 166.7 (CO_2CH_3). HRMS (EI): *m/z* [M^+] calcd for $C_{10}H_{10}O_5$: 210.0528; found: 210.0518.

*4.2.10. Dimethyl 2-(Thiophen-2-ylmethylene)malonate (**17f**)*

Following the method of preparation for **17a**, the reaction of **16f** (0.500 g, 4.46 mmol), **12b** (0.648 g, 4.91 mmol), piperidine (0.190 g, 2.23 mmol) and glacial AcOH (0.134 g, 2.23 mmol) yielded **17f** (0.728 g, 72%) as a yellow solid. R_f 0.59 (hexane/EtOAc, 7:3) mp 43-44 °C [Lit.[71] 43-44 °C]. IR (KBr): ῡ 3069, 1721, 1624, 1435, 1259, 1203, 1070, 935, 736 cm^{-1}. ^1H NMR (500 MHz, $CDCl_3$): δ 3.84 (s, 3H, CO_2CH_3), 3.94 (s, 3H, CO_2CH_3), 7.09 (dd, *J* = 5.0, 4.0 Hz, 1H, H-4"), 7.38 (dm, *J* = 4.0 Hz, 1H, H-3"), 7.55 (dt, 5.0, 1.0 Hz, 1H, H 5"), 7.90 (s, 1H, H-1'). ^{13}C NMR (125 MHz, $CDCl_3$): δ 52.6 (CO_2CH_3), 52.8 (CO_2CH_3), 121.4 (C-2), 127.8 (C-4"), 131.9 (C-5"), 134.8 (C-3"), 135.5 (C-1'), 135.9 (C-2"), 164.7 (CO_2CH_3), 166.6 (CO_2CH_3). HRMS (EI): m/z [M^+] calcd for $C_{10}H_{10}O_4S$: 226.0300; found: 226.0305.

*4.2.11. Dimethyl 2-(Pyridin-2-ylmethylene)malonate (**17g**)*

Following the method of preparation for **17a**, the reaction of **16g** (0.300 g, 2.80 mmol), **12b** (0.407 g, 3.08 mmol), piperidine (0.119 g, 1.40 mmol) and glacial AcOH (0.084 g, 1.40 mmol) afforded **17g** (0.470 g, 76%) as a reddish solid. R_f 0.38 (hexane/EtOAc, 9:1), mp 81-83 °C. IR (KBr): ῡ 2952, 1739, 1718, 1631, 1439, 1373, 1278, 1251, 1222, 1070, 946, 786 cm^{-1}. ^1H NMR (500 MHz, $CDCl_3$): δ 3.87 (s, 3H, CO_2CH_3), 3.91 (s, 3H,

CO_2CH_3), 7.26 (ddd, *J* = 8.0, 5.0, 1.5 Hz, 1H, H-5"), 7.39 (br d, *J* = 8.0 Hz, 1H, H-3"), 7.67 (s, 1H, H-1'), 7.72 (td, *J* = 8.0, 2.0 Hz, 1H, H-4"), 8.61 (br dd, *J* = 5.0, 1.5 Hz, 1H, H-6"). ^{13}C NMR (125 MHz, $CDCl_3$): δ 52.4 (CO_2CH_3), 52.8 (CO_2CH_3), 124.5 (C-5"), 126.3 (C-3"), 128.3 (C-2), 136.7 (C-4"), 139.9 (C-1'), 150.0 (C-6"), 151.0 (C-2"), 164.3 (CO_2CH_3), 167.0 (CO_2CH_3). MS (70 eV): m/z 221 (M^+, 4), 206 (M^+-15, 100), 190 (98), 160 (16), 155 (52), 149 (14), 122 (64), 91 (53). HRMS (EI): m/z [M+] calcd for $C_{11}H_{11}NO_4$: 221.0688; found: 221.0687.

*4.2.12. Dimethyl 2-((4-Nitrophenyl)(1H-pyrrol-2-yl)methyl)malonate (**18a**)*

After stirring a mixture of **17a** (0.300 g, 1.13 mmol) and I_2 (0.144 g, 0.57 mmol) in dry MeCN (30 mL) at room temperature for 5 min, **8b** (0.227 g, 3.39 mmol) was added, and stirred at room temperature for 12 h. Water (30 mL) was added, and the mixture extracted with EtOAc (3 x 40 mL). The organic layer was dried (Na_2SO_4) and the solvent removed under vacuum. The residue was purified by column chromatography over silica gel (20 g/g crude, hexane/EtOAc, 8:2) to obtain **18a** (0.295 g, 78%) as a pale yellow solid. R_f 0.38 (hexane/EtOAc, 7:3); mp 174-175 °C [Lit.[54] 170-171 °C]. IR (KBr): ῡ 3379, 3111, 2959, 1746, 1601, 1515, 1436, 1356, 1307, 1263, 1213, 1151, 861, 732, 703 cm^{-1}. ^{1}H NMR (500 MHz, $CDCl_3$): δ 3.53 (s, 3H, CO_2CH_3), 3.71 (s, 3H, CO_2CH_3), 4.21 (d, *J* = 10.0 Hz, 1H, H-2), 4.92 (d, *J* = 10.0 Hz, 1H, H-1'), 5.93-5.96 (m, 1H, H-3"), 6.10 (q, *J* = 2.5 Hz, 1H, H-4"), 6.69 (dt, *J* = 2.5, 1.5 Hz, 1H, H-5"), 7.41-7.46 (m, 2H, H-2'"), 8.13-8.17 (m, 2H, H-3'"), 8.57 (br s, 1H, NH). ^{13}C NMR (125 MHz, $CDCl_3$): δ 44.0 (C-1'), 52.8 (CO_2CH_3), 53.1 (CO_2CH_3), 57.2 (C-2), 107.2 (C-3"), 108.5 (C-4"), 118.3 (C-5"), 123.8 (C-3'"), 129.0 (C-2"), 129.1 (C-2'"), 147.0 (C-4'"), 147.3 (C-1'"), 167.5 (CO_2CH_3), 168.6 (CO_2CH_3). HRMS (EI): m/z [M+] calcd for $C_{16}H_{16}N_2O_6$: 332.1008; found: 332.1010.

*4.2.13. Dimethyl 2-((4-Cyanophenyl)(1H-pyrrol-2-yl)methyl)malonate (**18b**)*

Following the method of preparation for **18a**, the reaction of **17b** (0.300 g, 1.22 mmol), I_2 (0.154 g, 0.61 mmol) and **8b** (0.246 g, 3.67 mmol) in MeCN (30 mL) gave **18b** (0.295 g, 77%) as a brown solid. R_f 0.31 (hexane/EtOAc, 7:3); mp 166-167 °C. IR (KBr): ῡ 3345, 2959, 2232, 1751, 1606, 1433, 1356, 1301, 1262, 1216, 1177, 1148, 917, 858, 784, 726 cm^{-1}. ^{1}H NMR (300 MHz, $CDCl_3$): δ 3.52 (s, 3H, CO_2CH_3), 3.70 (s, 3H, CO_2CH_3), 4.19 (d, *J* = 10.4 Hz, 1H, H-2), 4.87 (d, *J* = 10.4 Hz, 1H, H-1'), 5.92-5.96 (m, 1H, H-3"), 6.09 (q, *J* =

2.7 Hz, 1H, H-4”), 6.68 (dt, *J* = 2.7, 1.5 Hz, 1H, H-5”), 7.36-7.41 (m, 2H, H-2’”), 7.55-7.60 (m, 2H, H-3’”), 8.60 (br s, 1H, N*H*). ^{13}C NMR (75.4 MHz, $CDCl_3$): δ 44.2 (C-1’), 52.8 (CO_2CH_3), 53.1 (CO_2CH_3), 57.0 (C-2), 106.9 (C-3”), 108.4 (C-4”), 111.1 (C-4’”), 118.2 (C-5”), 118.6 (CN), 128.9 (C-2’”), 129.1 (C-2”), 132.3 (C-3’”), 145.2 (C-1’”), 167.5 (CO_2CH_3), 168.6 (CO_2CH_3). HRMS (EI): m/z [M^+] calcd for $C_{17}H_{16}N_2O_4$: 312.1110; found: 312.1108.

*4.2.14. Dimethyl 2-((4-Bromophenyl)(1H-pyrrol-2-yl)methyl)malonate (**18c**)*

Following the method of preparation for **18a**, the reaction of **17c** (0.300 g, 1.00 mmol), I_2 (0.127 g, 0.50 mmol) and **8b** (0.201 g, 3.00 mmol) in MeCN (30 mL) furnished **18c** (0.108 g, 29%) as a pale yellow solid. R_f 0.30 (hexane/EtOAc, 8:2); mp 155-157 °C [Lit.[54] 158-160 °C]. IR (film): ῡ 3392, 2953, 1736, 1488, 1434, 1303, 1259, 1149, 1011, 725 cm^{-1}. ^{1}H NMR (500 MHz, $CDCl_3$): δ 3.51 (s, 3H, CO_2CH_3), 3.69 (s, 3H, CO_2CH_3), 4.14 (d, *J* = 10.5 Hz, 1H, H-2), 4.77 (d, *J* = 10.5 Hz, 1H, H-1’), 5.93 (br s, 1H, H-3”), 6.08 (q, *J* = 2.8 Hz, 1H, H-4”), 6.65-6.67 (m, 1H, H-5”), 7.13 (br d, *J* = 8.0, Hz, 2H, H-2’”), 7.41 (br d, *J* = 8.0 Hz, 2H, H-3’”), 8.46 (br s, 1H, N*H*). ^{13}C NMR (125 MHz, $CDCl_3$): δ 43.7 (C-1’), 52.6 (CO_2CH_3), 52.9 (CO_2CH_3), 57.4 (C-2), 106.6 (C-3”), 108.2 (C-4”), 117.9 (C-5”), 121.2 (C-4’”), 129.8 (C-2’”), 130.1 (C-2”), 131.7 (C-3’”), 138.8 (C-1’”), 167.7 (CO_2CH_3), 168.8 (CO_2CH_3). HRMS (EI): m/z [M^+] calcd for $C_{16}H_{16}BrNO_4$: 365.0263; found: 365.0258.

*4.2.15. Dimethyl 2-((3-Methoxyphenyl)(1H-pyrrol-2-yl)methyl)malonate (**18d**)*

Following the method of preparation for **18a**, the reaction of **17d** (0.300 g, 1.20 mmol), I_2 (0.091 g, 0.36 mmol) and **8b** (0.241 g, 3.60 mmol) in MeCN (30 mL) delivered **18d** (0.185 g, 49%) as a pale yellow solid. R_f 0.28 (hexane/EtOAc, 8:2); mp 103-105 °C. IR (film): ῡ 3397, 2954, 1733, 1600, 1586, 1490, 1435, 1259, 1154, 1034, 724 cm^{-1}. ^{1}H NMR (500 MHz, $CDCl_3$): δ 3.51 (s, 3H, CO_2CH_3), 3.69 (s, 3H, CO_2CH_3), 3.76 (s, 3H, OCH_3), 4.17 (d, *J* = 10.5 Hz, 1H, H-2), 4.78 (d, *J* = 10.5 Hz, 1H, H-1’), 5.95-5.97 (m, 1H, H-3”), 6.07 (q, *J* = 2.5 Hz, 1H, H-4”), 6.64 (dt, *J* = 2.5, 1.5 Hz, 1H, H-5”), 6.76 (br dd, *J* = 8.0, 0.5 Hz, 1H, H-4’”), 6.80 (t, *J* = 2.5 Hz, 1H, H-2’”), 6.85 (br d, *J* = 8.0 Hz, 1H, H-6’”), 7.21 (t, *J* = 8.0 Hz, 1H, H-5’”), 8.38 (br s, 1H, N*H*). ^{13}C NMR (125 MHz, $CDCl_3$): δ 44.3 (C-1’), 52.5 (CO_2CH_3), 52.8 (CO_2CH_3), 55.1 (OCH_3), 57.6 (C-2), 106.4 (C-3”), 108.1 (C-4”), 112.6 (C-4’”), 114.0 (C-2’”), 117.6 (H-5”), 120.3 (C-6’”), 129.6 (C-5’”), 130.6 (C-2”),

141.2 (C-1'''), 159.7 (C-3'''), 167.8 (CO_2CH_3), 168.9 (CO_2CH_3). HRMS (EI): m/z [M^+] calcd for $C_{17}H_{19}NO_5$: 317.1263; found: 317.1264.

*4.2.16. Dimethyl 2-(Furan-2-yl(1H-pyrrol-2-yl)methyl)malonate (**18e**).*

Following the method of preparation for **18a**, the reaction of **17e** (0.300 g, 1.43 mmol), $AlCl_3$ (0.096 g, 0.72 mmol) and 8b (0.288 g, 4.30 mmol) in MeCN (30 mL) provided **18e** (0.093 g, 24%) as a brown solid. R_f 0.33 (hexane/EtOAc, 7:3); mp 107-108 °C. IR (KBr): ῡ 3379, 2955, 1754, 1431, 1326, 1285, 1235, 1150, 1012, 913, 731 cm^{-1}. ^1H NMR (500 MHz, $CDCl_3$): δ 3.62 (s, 3H, CO_2CH_3), 3.65 (s, 3H, CO_2CH_3), 4.15 (d, J = 10.0 Hz, 1H, H-2), 4.90 (d, J = 10.0 Hz, 1H, H-1'), 6.01-6.02 (m, 1H, H-3'''), 6.08 (q, J = 3.0 Hz, 1H, H-4'''), 6.12 (dm, J = 3.0 Hz, 1H, H-3''), 6.28 (dd, J = 3.0, 1.5 Hz, 1H, H-4''), 6.70 (dt, J = 3.0, 1.5 Hz, 1H, H-5'''), 7.34 (dd, J = 1.5, 1.0 Hz, 1H, H-5''), 8.72 (br s, 1H, N*H*). ^{13}C NMR (125 MHz, $CDCl_3$): δ 38.2 (C-1'), 52.7 (CO_2CH_3), 52.8 (CO_2CH_3), 56.4 (C-2), 107.1 (C-3''), 107.4 (C-3'''), 108.1 (C-4'''), 110.4 (C-4''), 117.9 (C-5'''), 127.5 (C-2'''), 142.0 (C-5''), 152.7 (C-2''), 167.8 (CO_2CH_3), 168.4 (CO_2CH_3). HRMS (EI): m/z [M^+] calcd for $C_{14}H_{15}NO_5$: 277.0950; found: 277.0943.

*4.2.17. Dimethyl 2-((1H-Pyrrol-2-yl)(thiophen-2-yl)methyl)malonate (**18f**)*

Following the method of preparation for **18a**, the reaction of **17f** (0.300 g, 1.33 mmol), I_2 (0.170 g, 0.67 mmol) and **8b** (0.267 g, 3.99 mmol) in MeCN (30 mL) produced **18f** (0.205 g, 53%) as a brown solid. R_f 0.50 (hexane/EtOAc, 7:3), mp 121-123 °C. IR (KBr): ῡ 3385, 2951, 1752, 1434, 1342, 1277, 1234, 1142, 716 cm^{-1}. ^1H NMR (500 MHz, $CDCl_3$): δ 3.59 (s, 3H, CO_2CH_3), 3.67 (s, 3H, CO_2CH_3), 4.16 (d, J = 10.0Hz, 1H, H-2), 5.09 (d, J = 10.0 Hz, 1H, H-1'), 6.02-6.04 (m, 1H, H-3'''), 6.09 (q, J = 3.0 Hz, 1H, H-4'''), 6.68 (dt, J = 2.5, 1.5 Hz, 1H, H-5'''), 6.89 (ddd, J = 3.5, 1.5, 1.0 Hz, 1H, H-3''), 6.90 (dd, J = 5.0, 3.5 Hz, 1H, H-4''), 7.16 (dd, J = 5.0, 1.5 Hz, 1H, H-5''), 8.62 (br s, 1H, N*H*). ^{13}C NMR (125 MHz, $CDCl_3$): δ 39.6 (C-1'), 52.7 (CO_2CH_3), 52.8 (CO_2CH_3), 58.5 (C-2), 106.8 (C-3'''), 108.1 (C-4'''), 117.8 (C-5'''), 124.7 (C-5''), 125.3 (C-3''), 126.7 (C-4''), 129.9 (C-2'''), 143.3 (C-2''), 167.7 (CO_2CH_3), 168.5 (CO_2CH_3). HRMS (EI): m/z [M^+] calcd for $C_{14}H_{15}NO_4S$: 293.0722; found: 293.0730.

*4.2.18. Dimethyl 2-(Pyridin-2-yl(1H-pyrrol-2-yl)methyl)malonate (**18g**)*

Following the method of preparation for **18a**, the reaction of **17g** (0.300 g, 1.36 mmol), $AlCl_3$ (0.091 g, 0.68 mmol) and pyrrole (0.274 g, 4.08 mmol) in MeCN (30 mL) formed **18g** (0.248 g, 64%) as a pale yellow solid. R_f 0.36 (hexane/EtOAc, 9:1); mp 112-113 °C. IR (KBr): ῡ 3377, 2955, 1746, 1709, 1592, 1568, 1473, 1436, 1364, 1308, 1272, 1229, 1178, 1146, 923, 801, 723 cm^{-1}. ^1H NMR (500 MHz, $CDCl_3$): δ 3.56 (s, 3H, CO_2CH_3), 3.60 (s, 3H, CO_2CH_3), 4.52 (d, J = 10.0 Hz, 1H, H-2), 4.87 (d, J = 10.0 Hz, 1H, H-1'), 6.00-6.06 (m, 2H, H-3''', H-4'''), 6.69 (br, 1H, H-5'''), 7.12 (td, J = 5.0, 1.5 Hz, 1H, H-5''), 7.25 (br d, J = 7.5 Hz, 1H, H-3''), 7.58 (t, J = 7.5 Hz, 1H, H-4''), 8.53 (br d, J = 5.0 Hz, 1H, H-6''), 9.19 (br s, 1H, N*H*). ^{13}C NMR (125 MHz, $CDCl_3$): δ 45.5 (C-1'), 52.4 (CO_2CH_3), 53.6 (CO_2CH_3), 57.4 (C-2), 107.6 (C-3'''), 107.8 (C-4'''), 118.3 (C-5'''), 121.9 (C-5''), 124.0 (C-3''), 128.2 (C-2'''), 136.8 (C-4''), 148.9 (C-6''), 159.6 (C-2''), 168.3 (CO_2CH_3), 168.9 (CO_2CH_3). HRMS (EI): m/z [M^+] calcd for $C_{15}H_{16}N_2O_4$: 288.1110; found: 288.1108.

4.2.19. Methyl (1R,2S*)-1-(4-Nitrophenyl)-3-oxo-2,3-dihydro-1H-pyrrolizine-2-carboxylate (**19a**). Methyl (1R*,2R*)-1-(4-Nitrophenyl)-3-oxo-2,3-dihydro-1H-pyrrolizine-2-carboxylate (**20a**)*[54]

Compound **18a** (0.100 g, 0.30 mmol) was added to a solution of KOH (0.019 g, 0.33 mmol) in anhydrous THF (5 mL) under N_2 at 0 ºC, and the mixture was stirred at room temperature for 12 h. After adding water (30 mL), the mixture was extracted with EtOAc (3 x 20 mL). The organic layer was dried (Na_2SO_4) and the solvent removed under vacuum. The residue was purified by column chromatography over silica gel (10 g/g crude, hexane/EtOAc, 9:1) to generate a mixture of **19a**/**20a** (91:9) (0.070 g, 78%) as a red viscous oil. R_f 0.64 (hexane/EtOAc, 7:3). IR (film): ῡ 2919, 1760, 1735, 1519, 1402, 1348, 1292, 1243, 1164, 859, 722 cm^{-1}. ^1H NMR (500 MHz, $CDCl_3$): δ 3.89 (s, 3H, CO_2CH_3), 3.94 (d, J = 5.0 Hz, 1H, H-2), 5.06 (br d, J = 5.0 Hz, 1H, H-1), 6.03-6.05 (m, 1H, H-7), 6.57 (t, J = 3.0 Hz, 1H, H-6), 7.15 (br d, J = 3.0 Hz, 1H, H-5), 7.44-7.48 (m, 2H, H-2'), 8.20-8.24 (m, 2H, H-3'). Signals attributed to the minor isomer **20a**: δ 3.26 (s, CO_2CH_3), 4.51 (d, J = 9.0 Hz, H-1), 5.03 (br d, J = 9.0 Hz, H-1), 6.05-6.06 (m, H-7), 6.60 (t, J = 3.0 Hz, H-6), 7.21 (br d, J = 3.0 Hz, H-5), 7.38-7.42 (m, H-2'), 8.15-8.18 (m, H-3'). ^{13}C NMR (125 MHz, $CDCl_3$): δ 42.4 (C-1), 53.5 (CO_2CH_3), 61.6 (C-2), 106.9 (C-7), 112.5 (C-5), 120.2 (C-6), 124.4 (C-3'), 128.4 (C-2'), 138.3 (C-7a), 147.1 (C-1'), 147.6 (C-4'), 164.3 (C-3), 167.2

(CO_2CH_3). Signals attributed to the minor isomer **20a**: δ 112.5, 120.1, 123.6, 129.8. HRMS (EI): m/z [M^+] calcd for $C_{15}H_{12}N_2O_5$: 300.0746; found: 300.0749.

4.2.20. Methyl (1R,2S*)-1-(4-Cyanophenyl)-3-oxo-2,3-dihydro-1H-pyrrolizine-2-carboxylate (**19b**). Methyl (1R*,2R*)-1-(4-Cyanophenyl)-3-oxo-2,3-dihydro-1H-pyrrolizine-2-carboxylate (**20b**)*

Following the method of preparation for **19a**/**20a**, the reaction of **18b** (0.100 g, 0.32 mmol) and KOH (0.020 g, 0.35 mmol) in anhydrous THF (5 mL) resulted in a mixture of **19b**/**20b** (92:8) (0.059 g, 66%) as a red viscous oil. R_f 0.45 (hexane/EtOAc, 7:3). IR (film): ῡ 2290, 2228, 1760, 1735, 1608, 1467, 1403, 1292, 1243, 1164, 852, 724 cm^{-1}. ^1H NMR (500 MHz, $CDCl_3$): δ 3.88 (s, 3H, CO_2CH_3), 3.93 (d, J = 5.0 Hz, 1H, H-2), 5.01 (br d, J = 5.0 Hz, 1H, H-1), 6.01-6.03 (m, 1H, H-7), 6.56 (t, J = 3.0 Hz, 1H, H-6), 7.13 (br d, J = 3.0 Hz, 1H, H-5), 7.39-7.42 (m, 1H, H-2'), 7.65-7.68 (m, 1H, H-3'). Signals attributed to the minor isomer **20b**: δ 3.24 (s, CO_2CH_3), 4.49 (d, J = 9.0 Hz, H-1), 4.98 (br d, J = 9.0 Hz, H-1), 6.04-6.05 (m, H-7), 6.59 (t, J = 3.3 Hz, H-6), 7.20 (br d, J = 3.3 Hz, H-5), 7.33-7.35 (m, H-2'), 7.61-7.63 (m, H-3'). ^{13}C NMR (125 MHz, $CDCl_3$): δ 42.6 (C-1), 53.5 (CO_2CH_3), 61.6 (C-2), 106.8 (C-7), 111.9 (C-4'), 112.3 (C-5), 118.3 (CN), 120.2 (C-6), 128.2 (C-2'), 132.9 (C-3'), 138.4 (C-7a), 145.2 (C-1'), 164.4 (C-3), 167.2 (CO_2CH_3). Signals attributed to the minor isomer **20b**: δ 42.0, 52.0, 62.0, 129.6, 132.0. HRMS (EI): m/z [M^+] calcd for $C_{16}H_{12}N_2O_3$: 280.0848; found: 280.0857.

4.2.21. Methyl (1R,2S*)-1-(4-Bromophenyl)-3-oxo-2,3-dihydro-1H-pyrrolizine-2-carboxylate (**19c**). Methyl (1R*,2R*)-1-(4-Bromophenyl)-3-oxo-2,3-dihydro-1H-pyrrolizine-2-carboxylate (**20c**)[54]*

Following the method of preparation for **19a**/**20a**, the reaction of **18c** (0.100 g, 0.27 mmol) and KOH (0.017 g, 0.30 mmol) in anhydrous THF (5 mL) yielded a mixture of **19c**/**20c** (90:10) (0.052 g, 57%) as a red viscous oil. R_f 0.64 (hexane/EtOAc, 7:3). IR (film): ῡ 1761, 1737, 1489, 1470, 1405, 1297, 1244, 1166, 1011, 850, 725 cm^{-1}. ^1H NMR (500 MHz, $CDCl_3$): δ 3.85 (s, 3H, CO_2CH_3), 3.90 (d, J = 5.0 Hz, 1H, H-2), 4.89 (br d, J = 5.0 Hz, 1H, H-1), 5.95-6.00 (m, 1H, H-7), 6.54 (t, J = 3.5 Hz, 1H, H-6), 7.11 (dt, J = 3.5, 0.5 Hz, 1H, H-5), 7.13 (dm, J = 8.5 Hz, 2H, H-2'), 7.47 (dm, J = 8.5 Hz, 2H, H-3'). Signals attributed to the minor isomer **20c**: δ 3.25 (s, CO_2CH_3), 4.43 (d, J = 9.5 Hz, H-1), 6.00-6.02

(m, H-7), 6.56 (t, *J* = 3.5 Hz, H-6), 7.07 (dm, *J* = 8.5 Hz, H-2'), 7.43 (dm, *J* = 8.5 Hz, H-3'). ^{13}C NMR (125 MHz, $CDCl_3$): δ 42.3 (C-1), 53.3 (CO_2CH_3), 62.0 (C-2), 106.5 (C-7), 112.0 (C-5), 120.1 (C-6), 121.8 (C-4'), 129.0 (C-2'), 132.2 (C-3'), 138.9 (C-1'), 139.4 (C-7a), 165.0 (C-3), 167.5 (CO_2CH_3). Signals attributed to the minor isomer **20c**: δ 41.7 (C-1), 52.2 (CO_2CH_3), 59.2 (C-2), 106.6 (C-7), 112.1 (C-5), 120.0 (C-6), 130.4 (C-2'), 131.4 (C-3'). HRMS (EI): m/z [M^+] calcd for $C_{15}H_{12}BrNO_3$: 333.0001; found: 333.0000.

4.2.22. Methyl (1R,2S*)-1-(3-Methoxyphenyl)-3-oxo-2,3-dihydro-1H-pyrrolizine-2-carboxylate (**19d**). Methyl (1R*,2R*)-1-(3-Methoxyphenyl)-3-oxo-2,3-dihydro-1H-pyrrolizine-2-carboxylate (**20d**)*

Following the method of preparation for **19a**/**20a**, the reaction of **18d** (0.100 g, 0.32 mmol) and KOH (0.019 g, 0.35 mmol) in anhydrous THF (5 mL) furnished a mixture of **19d**/**20d** (90:10) (0.052 g, 57%) as a red viscous oil. R_f 0.66 (hexane/EtOAc, 7:3). IR (film): ῡ 2954, 1761, 1737, 1601, 1490, 1467, 1436, 1404, 1292, 1267, 1164, 1048, 725 cm^{-1}. ^{1}H NMR (500 MHz, $CDCl_3$): δ 3.78 (s, 3H, OCH_3), 3.85 (s, 3H, CO_2CH_3), 3.97 (d, *J* = 5.0 Hz, 1H, H-2), 4.89 (br d, *J* = 5.0 Hz, 1H, H-1), 6.00-6.01 (m, 1H, H-7), 6.53 (t, *J* = 3.0 Hz, 1H, H-6), 6.78 (br t, *J* = 1.5 Hz, 1H, H-2'), 6.82-8.85 (m, 2H, H-4', H-6'), 7.10 (dm, *J* = 3.0 Hz, 1H, H-5), 7.26 (t, *J* = 7.5 Hz, 1H, H-5'). Signals attributed to the minor isomer **20d**: δ 3.24 (s, CO_2CH_3), 4.43 (d, *J* = 9.5 Hz, H-1), 6.03-6.05 (m, H-7), 6.57 (t, *J* = 3.0 Hz, H-6), 6.72-6.74 (m, H-2'), 7.16-7.18 (m, H-5), 7.22 (t, *J* = 8.0 Hz, H-5'). ^{13}C NMR (125 MHz, $CDCl_3$): δ 42.9 (C-1), 53.3 (CO_2CH_3), 55.2 (OCH_3), 62.1 (C-2), 106.4 (C-7), 111.8 (C-5), 112.9 (C-4'), 113.2 (C-2'), 119.5 (C-6'), 120.0 (C-6), 130.1 (C-5'), 139.9 (C-7a), 141.5 (C-1'), 160.0 (C-3'), 165.3 (C-3), 167.7 (CO_2CH_3). HRMS (EI): m/z [M^+] calcd for $C_{16}H_{15}NO_4$: 285.1001; found: 285.1002.

4.2.23. Methyl (1R,2R*)-1-(2-Furan-yl)-3-oxo-2,3-dihydro-1H-pyrrolizine-2-carboxylate (**19e**). Methyl (1R*,2S*)-1-(2-Furan-yl)-3-oxo-2,3-dihydro-1H-pyrrolizine-2-carboxylate (**20e**)*

Following the method of preparation for **19a**/**20a**, the reaction of **18e** (0.100 g, 0.36 mmol) and KOH (0.022 g, 0.40 mmol) in anhydrous THF (5 mL) afforded a mixture of **19e**/**20e** (92:8) (0.072 g, 80%) as a red viscous oil. R_f 0.67 (hexane/EtOAc, 7:3 x 2). IR (film): ῡ 2955, 1763, 1737, 1469, 1404, 1297, 1246, 1220, 1165, 1010, 727 cm^{-1}. ^{1}H NMR

(500 MHz, $CDCl_3$): δ 3.87 (s, 3H, CO_2CH_3), 4.17 (d, *J* = 5.0 Hz, 1H, H-2), 5.00 (br d, *J* = 5.0 Hz, 1H, H-1), 6.10-6.12 (m, 1H, H-7), 6.23 (dt, *J* = 3.5, 1.0 Hz, 1H, H-3'), 6.32 (dd, *J* = 3.5, 2.0 Hz, 1H, H-4'), 6.52 (t, *J* = 3.5 Hz, 1H, H-6), 7.08 (dt, *J* = 3.5, 0.5 Hz, 1H, H-5), 7.37 (dd, *J* = 2.0, 1.0 Hz, 1H, H-5'). Signals attributed to the minor isomer **20e**: δ 3.47 (s, CO_2CH_3), 4.39 (d, *J* = 9.0 Hz, H-1), 6.12-6.13 (m, H-7), 6.22 (dt, *J* = 3.5, 0.5 Hz, H-3'), 6.55 (t, *J* = 3.5 Hz, H-6), 7.15 (dt, *J* = 3.5, 1.0 Hz, H-5). ^{13}C RMN (125 MHz, $CDCl_3$): δ 36.6 (C-1), 53.3 (CO_2CH_3), 58.8 (C-2), 106.3 (C-7), 106.8 (C-3'), 110.4 (C-4'), 112.1 (C-5), 119.9 (C-6), 137.4 (C-7a), 142.8 (C-5'), 151.6 (C-2'), 164.9 (C-3), 167.4 (CO_2CH_3). HRMS (EI): m/z [M^+] calcd for $C_{13}H_{11}NO_4$: 245.0688; found: 245.0693.

4.2.24. Methyl (1R,2R*)-3-Oxo-1-(2-thiophen-yl)-2,3-dihydro-1H-pyrrolizine-2-carboxylate (**19f**). Methyl (1R*,2S*)-3-Oxo-1-(2-thiophen-yl)-2,3-dihydro-1H-pyrrolizine-2-carboxylate (**20f**)*

Following the method of preparation for **19a**/**20a**, the reaction of **18f** (0.100 g, 0.34 mmol) and KOH (0.021 g, 0.37 mmol) in anhydrous THF (5 mL) gave a mixture of **19f**/**20f** (93:7) (0.059 g, 66%) as a red viscous oil. R_f 0.71 (hexane/EtOAc, 7:3). IR (film): ῡ 2954, 1761, 1574, 1469, 1403, 1298, 1243, 1163, 1086, 975, 853, 710 cm^{-1}. ^{1}H NMR (500 MHz, $CDCl_3$): δ 3.87 (s, 3H, CO_2CH_3), 4.05 (d, *J* = 5.0 Hz, 1H, H-2), 5.22 (br d, *J* = 5.0 Hz, 1H, H-1), 6.13-6.16 (m, 1H, H-7), 6.54 (t, *J* = 3.0 Hz, 1H, H-6), 6.97 (dd, *J* = 5.0, 3.5 Hz, 1H, H-4'), 7.01 (dm, *J* = 3.5 Hz, 1H, H-3'), 7.10 (br d, *J* = 3.0, Hz, 1H, H-5), 7.24 (dd, *J* = 5.0, 1.5 Hz, 1H, H-5'). Signals attributed to the minor isomer **20f**: δ 3.36 (s, CO_2CH_3), 4.42 (d, *J* = 9.0 Hz, H-1), 6.56 (t, *J* = 3.0 Hz, H-6), 7.16 (br d, *J* = 3.0, Hz, H-5). ^{13}C NMR (125 MHz, $CDCl_3$): δ 38.1 (C-1), 53.3 (CO_2CH_3), 62.4 (C-2), 106.7 (C-7), 112.0 (C-5), 119.9 (C-6), 125.0 (C-5'), 125.4 (C-3'), 127.1 (C-4'), 139.3 (C-7a), 142.6 (C-2'), 164.7 (C-3), 167.4 (CO_2CH_3). HRMS (EI): m/z [M^+] calcd for $C_{13}H_{11}NO_3S$: 261.0460; found: 261.0461.

4.2.25. Methyl (1R,2R*)-3-Oxo-1-(2-pyridin-2-yl)-2,3-dihydro-1H-pyrrolizine-2-carboxylate (**19g**). Methyl (1R*,2S*)-3-Oxo-1-(pyridin-2-yl)-2,3-dihydro-1H-pyrrolizine-2-carboxylate (**20g**)*

Following the method of preparation for **19a**/**20a**, the reaction of **18g** (0.100 g, 0.35 mmol) and KOH (0.021 g, 0.38 mmol) in anhydrous THF (5 mL) provided a mixture of **19g**/**20g** (93:7) (0.062 g, 70%) as a red viscous oil. R_f 0.69 (hexane/EtOAc, 7:3 x 2). IR

(film): ῡ 2954, 1762, 1736, 1591, 1572, 1469, 1435, 1403, 1293, 1244, 1163, 721 cm^{-1}. ^1H NMR (500 MHz, $CDCl_3$): δ 3.85 (s, 3H, CO_2CH_3), 4.69 (br d, *J* = 5.0 Hz, 1H, H-2), 5.04 (br d, *J* = 5.0 Hz, 1H, H-1), 5.96-5.98 (m, 1H, H-7), 6.46-6.49 (m, 1H, H-6), 7.07-7.09 (m, 1H, H-5), 7.19-7.23 (m, 1H, H-5'), 7.36 (br d, *J* = 7.5 Hz, 1H, H-3'), 7.69 (tm, *J* = 7.5 Hz, 1H, H-4'), 8.56 (brd, *J* = 5.0 Hz, 1H, H-6'). Signals attributed to the minor isomer **20g**: δ 3.74 (s, CO_2CH_3), 4.56 (dm, *J* = 9.3 Hz, H-1), 5.11 (br d, *J* = 9.3 Hz, H-1), 8.53 (br d, *J* = 4.0 Hz, H-6'). ^{13}C NMR (125 MHz, $CDCl_3$): δ 44.5 (C-1), 53.2 (CO_2CH_3), 58.8 (C-2), 105.8 (C-7), 111.9 (C-5), 119.7 (C-6), 122.2 (C-3'), 122.7 (C-5'), 137.0 (C-4'), 139.5 (C-7a), 150.0 (C-6'), 158.0 (C-2'), 165.7 (C-3), 168.0 (CO_2CH_3). HRMS (EI): m/z [M^+] calcd for $C_{14}H_{12}N_2O_3$: 256.0848; found: 256.0836.

*4.2.26. Methyl 1-(4-Nitrophenyl)-3-oxo-3H-pyrrolizine-2-carboxylate (**21a**)*

Method A. In a threaded ACE glass pressure tube with a sealed Teflon screw cap and magnetic stirring bar, a mixture of **19a**/**20a** (0.025 g, 0.08 mmol) was dissolved in THF (1.0 mL) before adding a solution of NaOMe in MeOH (1.0 M) (0.009 g, 0.16 mmol) at room temperature. The reaction mixture was heated to 50 °C for 2 h, diluted with EtOAc (20 mL) and washed with a 5% aqueous solution of HCl (3.0 mL) and water (5.0 mL). The organic layer was dried (Na_2SO_4) and the solvent removed under vacuum. The residue was purified by column chromatography over silica gel (20 g/g crude, hexane/EtOAc, 9:1) to afford **21a** (0.010 g, 42%) as a reddish solid. R_f 0.41 (hexane/EtOAc, 7:3); mp 158–160 °C.

Method B. A mixture of **19a**/**20a** (0.055 g, 0.18 mmol) and DDQ (0.082 g, 0.36 mmol) in dry CH_2Cl_2 (6.0 mL) was stirred in an open flask at room temperature for 12 h. After filtration through celite, the solvent was removed under vacuum. The residue was purified by column cromatography over silica gel (20 g/g crude, hexane/EtOAc, 9:1) to deliver **21a** (0.025 g, 46%) as a reddish solid. R_f 0.41 (hexane/EtOAc, 7:3); mp 158–160 °C. IR (film): ῡ 2918, 1751, 1708, 1545, 1520, 1351, 1213, 1143, 1014, 856, 743 cm^{-1}. ^1H NMR (600 MHz, $CDCl_3$) δ 3.79 (s, 3H, CO_2CH_3), 6.22 (t, *J* = 3.0 Hz, 1H, H-6), 6.30 (d, *J* = 3.0 Hz, 1H, H-7), 7.17 (d, *J* = 3.0 Hz, 1H, H-5), 7.80–7.83 (m, 2H, H-2'), 8.31–8.36 (m, 2H, H-3'). ^{13}C NMR (150 MHz, $CDCl_3$) δ 52.1 (CO_2CH_3), 116.9 (C-7), 117.0 (C-6), 118.0 (C-2), 121.6 (C-5), 123.5 (C-3'), 130.0 (C-2'), 134.6 (C-7a), 136.5 (C-1'), 149.2 (C-4'), 155.2 (C-

1), 160.7 (C-3), 161.7 (CO_2CH_3). HRMS (EI): m/z [M^+] calcd for $C_{15}H_{10}N_2O_5$: 298.0590; found: 298.0591.

*4.2.27. Methyl 1-(4-bromophenyl)-3-oxo-3H-pyrrolizine-2-carboxylate (**21b**)*

Following the method B of preparation for **21a**, the reaction of a mixture of **19c**/**20c** (0.090 g, 0.27 mmol) and DDQ (0.154 g, 0.68 mmol) in dry CH_2Cl_2 (2.0 mL) produced **21b** (0.062 g, 70%) as a reddish solid. R_f 0.62 (hexane/EtOAc, 7:3); mp 131–133 °C. IR (film): ῡ 2951, 1748, 1710, 1589, 1541, 1435, 1406, 1348, 1210, 1144, 1011, 837, 745 cm^{-1}. ^1H NMR (600 MHz, $CDCl_3$) δ 3.79 (s, 3H, CO_2CH_3), 6.19 (t, *J* = 3.0 Hz, 1H, H-6), 6.30 (dd, *J* = 3.0, 0.6 Hz, 1H, H-7), 7.14 (dd, *J* = 3.0, 0.6 Hz, 1H, H-5), 7.54–7.57 (m, 2H, H-2'), 7.61–7.63 (m, 2H, H-3'). ^{13}C NMR (150 MHz, $CDCl_3$) δ 51.9 (CO_2CH_3), 116.4 (C-2), 116.56 (C-7), 116.61 (C-6), 120.9 (C-5), 126.2 (C-4'), 129.2 (C-1'), 130.6 (C-2'), 131.7 (C-3'), 134.8 (C-7a), 156.5 (C-1), 161.4 (C-3), 162.2 (CO_2CH_3). HRMS (EI): m/z [M^+] calcd for $C_{15}H_{10}BrNO_3$: 330.9844; found: 330.9846.

4.3. Anti-inflammatory activity

The anti-inflammatory activity of the test compounds was evaluated with 7- to 8-weeks old male CD1 mice, which were randomly assigned to groups (n = 7). The mice were housed in hanging metal cages (three per each cage) and maintained at a temperature of 24 ± 2 °C and 45% relative humidity, on a 12/12 h light/dark cycle. All animals were handled and all procedures carried out in accordance with ethical principles and regulations specified by the Bioethics Committee of our Institution and the standards of the National Institutes of Health of Mexico.

4.3.1. TPA-induced ear edema

In the first phase of the experiment, all animals received a local topical application of TPA (2.5 µg) in 25 µl of acetone over the right ear (Wu) and 25 µl of acetone (Wo) only over the left ear. This was the only treatment given to the control group. Thirty minutes after the administration of TPA, 2 mg of one of the test compounds or of indomethacin was applied on the right ear (Ws) of the mice in the experimental groups. At 6 h post-administration of the anti-inflammatory agent, animals were euthanized and then sacrificed by cervical

dislocation. Ear sections 6 mm in diameter were obtained to determine the degree of inflammation, with the value for the TPA control (untreated with an anti-inflammatory agent) as 100% inflammation. Calculation of the inhibition of inflammation was based on the weight difference between right and left ear sections, according to the following formula: % Inhibition = [(Wu-Wo) TPA control – (Ws-Wo) TPA treated/(Wu-Wo) TPA control] x 100.[26,58]

In a second phase of the experiment, the compounds showing anti-inflammatory activity statistically similar to that of indomethacin were subjected to additional assays. They were evaluated at three doses (0.5, 1.0 and 2.0 mg/ear) to find the ED_{50} in each compound, using the procedure already described for the determination of the percentage of inflammation.

4.3.2. *Statistics*

Data are expressed as the mean ± the standard error of the mean (SEM). Statistical significance was examined with one-way analysis of variance (ANOVA) followed by the Student-Newman-Keuls post-hoc test,[72] on Graph Pad Prism 5.00 software.[73] The p-values given in the tables and figures refer to the differences between the experimental and corresponding control value, with significance considered at $p \leq 0.05$.

4.4. Docking

4.4.1. Protein and ligand structures

The crystallographic structure of human cyclooxygenase-2 (COX-2) complexed with a selective inhibitor 1-phenylsulfonamide-3-trifluoromethyl-5-parabromophenylpyrazole (SC558) was retrieved from the Protein Data Bank (PDB) (http://www.rcsb.org/), with the code 1CX2.[60] The docking validation was carried out with SC-558 to identify the main side chains present in the active site of the enzyme. Before docking runs were made, the coordinates of the protein were set, water molecules were removed, hydrogen atoms were added to the polar atoms (considering pH at 7.4), and Kollman charges were assigned. The 3D structures of indomethacin were downloaded from the Zinc database.[74] The structures of the ligands were sketched in two dimensions (2D) with ChemSketch (https://www.acdlabs.com/resources/freeware/chemsketch/) and optimized with AM1 on

Gaussian 98[75] software in order to obtain the minimum energy conformation for the docking studies.

4.4.2. Molecular docking studies

The protein-ligand interaction was observed on AutoDock and AutoDockTools.[59] All the possible rotatable bonds, torsion angles, atomic partial charges and non-polar hydrogens were determined for each ligand. For subunit A of COX-2, the grid dimensions in AutoDockTools were 72 x 60 x 70 $Å^3$ with points separated by 0.375 Å, centered at: X = 24.471, Y = 22.312 and Z = 15.999. The hybrid Lamarckian genetic algorithm was applied for minimization, utilizing default parameters. A total of one hundred docking runs were conducted, adopting the conformation with the lowest binding energy (kcal/mol) for all further simulations. AutoDockTools was used to prepare the script and files as well as to visualize the docking results, which were edited in Discovery 4.0 Client.[76]

4.5. COX-2 enzyme and nitric oxide inhibitory activity

4.5.1. Cell viability assay

Cell viability was assessed with a modified 3-(4,5-dimethylthiazol-2-yl)-2,5-diphenyl-2*H*-tetrazolium bromide (MTT) assay.[64] J774A.1 macrophages (8×10^4 cells/well) were seeded in Dulbecco's Modified Eagle's Medium (DMEM) in a 96 well plate and treated with the mixtures **19a**/**20a**, **19b**/**20b** and **19c**/**20c** at a concentration of 6.25, 12.5, 25.0, 50.0, 100.0, 150.0 and 200.0 µg/mL dissolved in DMSO. After 48 h of exposure, 10 µL of MTT solution (5 mg/mL in phosphate-buffered saline) were added to each well, and the plate was incubated at 37 °C for 4 h. Subsequently, the medium was removed, and the formazan crystals were dissolved in 100 µL of DMSO. The optical density (OD) was quantified at 540 nm on an ELISA plate reader from BioRad. Six replicate wells were used to calculate viability with the following equation:

$$\% \text{ Viability} = \frac{OD_{\text{treated cells}}}{OD_{\text{control cells}}} \times 100$$

4.5.2. Determination of nitric oxide production

The level of nitrites was evaluated by the Griess reaction.[69] The J774A.1 macrophages (1×10^6 cells/well) were treated with **19a**/**20a**, **19b**/**20b**, **19c**/**20c** or indomethacin at 25

μg/mL, and then incubated for 2 h. Lipopolysaccharide (LPS, *Escherichia coli* O111:B4, 5 μg/mL) was added and the cells were incubated for another 24 h. Afterwards, the supernatant was collected and 100 μL were exposed to 100 μL of the Griess reagent (Sigma-Aldrich). The mixture was incubated at 37 °C for 15 min before measuring absorbance at 540 nm on a microplate reader.

4.5.3. RT-PCR Analysis of mRNA

The J774A.1 macrophages (2 × 10^6 cells/well) were cultured in 12-well plates with **19a**/**20a**, **19b**/**20b** or **19c**/**20c** (25 μg/mL) for 2 h. Then, they were stimulated with LPS (5 μg/mL), and incubated for 24 h.[77] The inhibitory effect of the epimers on mRNA expression of COX-2 was determined by semiquantitative RT-PCR. The PCR products were normalized to the amount of 18S ribosomal RNA. Primers were designed with Primer BLAST (http://www.ncbi.nlm.nih.gov/tools/primer-blast/) (Table 6).

Table 6. List of sequences used for RT-PCR

Gene	Sequence	Length (bP)
COX-2	Forward GCG AGC TAA GAG CTT CAG GA	212
	Reverse TCA TAC ATT CCC CAC GGT TT	

Conflict of interest

The authors declare that they have no conflict of interest.

Acknowledgments

We thank Dr. Enrique Herbert-Pucheta for NMR experimental assistance and Bruce A. Larsen for proofreading the manuscript. O.G.-G., F.D. and J.T. gratefully acknowledge the Secretaría de Investigación y Posgrado (SIP)-IPN (Grants 20160791, 20170902, 20181332, 20180198, 20181966, 20195228 and 20195287) and CONACYT (Grants 178319, 282033

and A1-S-17131) for financial support. D.A.M., C.H.E., G.A.G.-R., and R.I.H.-B. are thankful to CONACYT for graduate scholarships awarded and also to SIP-IPN (PIFI) for scholarship complements. G.A.C.-C., F.D. and J.T. are fellows of the Estímulos al Desempeño de los Investigadores (EDI)-IPN and Comisión de Operación y Fomento de Actividades Académicas (COFAA)-IPN programs.

Appendix A. Supplementary data

Supplementary data to this article can be found online at http://doi.org/10.1016/j.bmc.

References

1. Afonina IS, Zhong Z, Karin M, Beyaert R. Limiting inflammation–the negative regulation of NF-κB and the NLRP3 inflammasome. *Nature Immunol.* 2017;18:861–869. https://doi.org/10.1038/ni.3772.
2. Manthiram K, Zhou Q, Aksentijevich I, Kastner DI. The monogenic autoinflammatory diseases define new pathways in human innate immunity and inflammation. *Nature Immunol.* 2017;18:832–842. https://doi.org/10.1038/ni.3777.
3. Sherwood ER, Toliver-Kinsky T. Mechanisms of the inflammatory response. *Best Pract Res Clin Anaesthesiol.* 2004;18: 385–405. https://doi.org/10.1016/j.bpa.2003.12.002.
4. Zitvogel L, Pietrocola F, Kroemer G. Nutrition, inflammation and cancer. *Nature Immunol.* 2017;18:843–850. https://doi.org/10.1038/ni.3754.
5. Pourtarzam M, Zadhoush F, Sadeghi M. The difference in correlation between insulin resistance index and chronic inflammation in type 2 diabetes with and without metabolic syndrome. *Adv Biomed Res.* 2016;5:153. http://doi.org/10.4103/2277-9175.188489.
6. Golia E, Limongelli G, Natale F, Fimiani F, Maddaloni V, Pariggiano I, Bianchi R, Crisci M, D'Acierno L, Giordano R, Di Palma G, Conte M, Golino P, Russo MG, Calabrò R, Calabrò P. Inflammation and cardiovascular disease: From pathogenesis to therapeutic target. *Curr Atheroscler Rep.* 2014;16:435. https://doi.org/10.1007/s11883-014-0435-z.
7. Lopez-Candales A, Hernández Burgos PM, Hernandez-Suarez DF, Harris D. Linking chronic inflammation with cardiovascular disease: From normal aging to the metabolic syndrome. J Nat Sci. 2017;3:e341. https://www.jnsci.org/content/341.

8. Amor A, Puentes F, Baker D, van der Valk P. Inflammation in neurodegenerative diseases. *Immunology* 2010;129:154–169. https://doi.org/10.1111/j.1365-2567.2009.03225.x.
9. Wu P-P, He H, Hong WD, Wu T-R, Huang G-Y, Zhong Y-Y, Tu B-R, Gao M, Zhou J, Zhao S-Q, Li D-L, Xu X-T, Sheng Z-J, Ward SA O'Neill PM, Zhang K. The biological evaluation of fusidic acid and its hydrogenation derivative as antimicrobial and anti-inflammatory agents. *Infect Drug Resist.* 2018;11:1945–1957. http://doi.org/10.1101/311951.
10. Cryer B. NSAID-associated deaths: The rise and fall of NSAID-associated GI mortality. *Am J Gastroenterol.* 2005;100:1694–1695. https://doi.org/10.1111/j.1572-0241.2005.50565.x
11. Singh G. Recent considerations in nonsteroidal anti-inflammatory drug gastropathy. *Am J Med.* 1998;105:31S–38S. https://doi.org/10.1016/S0002-9343(98)00072-2.
12. Massó González EL, Patrignani P, Tacconelli S, García Rodríguez LA. Variability among nonsteroidal antiinflammatory drugs in risk of upper gastrointestinal bleeding. *Arthritis Rheumatol.* 2010;62:1592–1601. https://doi.org/10.1002/art.27412.
13. Schneider V, Lévesque LE, Zhang B, Hutchinson T, Brophy JM. Association of selective and conventional nonsteroidal antiinflammatory drugs with acute renal failure: A population-based, nested case-control analysis. *Am J Epidemiol.* 2006;164:881–889. https://doi.org/10.1093/aje/kwj331.
14. García Rodríguez LA, Tacconelli S, Patrignani P. Role of dose potency in the prediction of risk of myocardial infarction associated with nonsteroidal anti-inflammatory drugs in the general population. *J Am Coll Cardiol.* 2008;52:1628–1636. https://doi.org/10.1016/j.jacc.2008.08.041.
15. Gür ZT, Çalişkan B, Banoglu E. Drug discovery approaches targeting 5-lipoxygenase-activating protein (FLAP) for inhibition of cellular leukotriene biosynthesis. *Eur J Med Chem.* 2018;153:34–48. https://doi.org/10.1016/j.ejmech.2017.07.019.
16. Gouda AM, Abdelazeem AH. An integrated overview on pyrrolizines as potential anti-inflammatory, analgesic and antipyretic agents. *Eur J Med Chem.* 2016;114:257–292. https://doi.org/10.1016/j.ejmech.2016.01.055.
17. Tries S, Laufer S. The pharmacological profile of ML3000: A new pyrrolizine derivative inhibiting the enzymes cyclo-oxygenase and 5-lipoxygenase. *Inflammopharmacology.* 2001;9:113–124. https://doi.org/10.1163/156856001300248380.
18. Vidal C; Gómez-Hernández A, Sánchez-Galán E, González A, Ortega L, Gómez-Gerique JA, Tuñón J, Egido J. Licofelone, a balanced inhibitor of cyclooxygenase and 5-lipoxygenase, reduces inflammation in a rabbit model of atherosclerosis. *J Pharmacol Exp Ther.* **2007**, *320*, 108–116. https://doi.org/10.1124/jpet.106.110361.

19. Liu W, Zhou J, Zhang H, Qian H, Yin J, Bensdorf K, Gust R. Synthesis and biological evaluation of licofelone derivatives as anticancer and anti-inflammatory agents. *Lett Drug Des Discov.* 2011;8:911–917. https://doi.org/10.2174/157018011797655223.
20. Muchowski JM, Cooper GF, Halpern O, Koehler R, Kluge AF, Simon RL, Unger SH, Van Horn AR, Wren DL, Ackrell J, et al. Synthesis and antiinflammatory and analgesic activity of 5-aroyl-1,2-dihydro-3*H*-pyrrolo[1,2-*a*]pyrrole-1-carboxylic acids. The 6-substituted compounds. *J Med Chem.* 1987;30:820–823. https://pubs.acs.org/doi/pdf/10.1021/jm00388a013.
21. Fiorucci S, Meli R, Bucci M, Cirino G. Dual inhibitors of cyclooxygenase and 5-lipoxygenase. A new avenue in anti-inflammatory therapy? *Biochem Pharmacol.* 2001;62:1433–1438. https://doi.org/10.1016/S0006-2952(01)00747-X
22. Vacha ME. The role of subcutaneous ketorolac for pain management. *Hosp Pharm.* 2015;50:108–112. https://doi.org/10.1310/hpj5002-108.
23. Bucley MM-T, Brogden RN. Ketorolac: A review of its pharmacodynamic and pharmacokinetic properties and therapeutic potential. *Drugs* 1990;39:86–109. https://doi.org/10.2165/00003495-199039010-00008.
24. Gillis JC, Brogden RN. Ketorolac- A reappraisal of its pharmacodynamic and pharmacokinetic properties and therapeutic use in pain management. *Drugs* 1997;53:139–188. https://doi.org/10.2165/00003495-199753010-00012.
25. Maguire AR, Plunkett SJ, Papot S, Clynes M, O'Connor R, Touhey S. Synthesis of indomethacin analogues for evaluation as modulators of MRP activity. *Bioorg Med Chem.* 2001;9:745–762. https://doi.org/10.1016/S0968-0896(00)00292-3.
26. Gómez-Rivera A, González-Cortazar M, Herrera-Ruiz M, Zamilpa A, Rodríguez-López V. Sessein and isosessein with anti-inflammatory, antibacterial and antioxidant activity isolated from *Salvia sessei* Benth. *J Ethnopharmacol.* 2018;217:212–219. https://doi.org/10.1016/j.jep.2018.02.012.
27. Gómez M, Gil JF. Topical anti-inflammatory activity of *Calea prunifolia* HBK (Asteraceae) in the TPA model of mouse ear inflammation. *J Braz Chem Soc.* 2011;22:2391–2395. http://dx.doi.org/10.1590/S0103-50532011001200021.
28. Del-Ángel M, Nieto A, Ramírez-Apan T, Delgado G. Anti-inflammatory effect of natural and semi-synthetic phthalides. *Eur J Pharmacol.* 2015;752:40–48. https://doi.org/10.1016/j.ejphar.2015.01.026.
29. Ulbrich H, Fiebich B, Dannhardt G. Cyclooxygenase-1/2 (COX-1/COX-2) and 5-lipoxygenase (5-LOX) inhibitors of the 6,7-diaryl-2,3-1H-dihydropyrrolizine type. *Eur J Med Chem.* 2002;37:953–959. https://doi.org/10.1016/S0223-5234(02)01418-6.

30. Laufer S, Striegel H-G, Neher K, Zechmeister P, Donat C, Stolingwa K, Baur S, Tries S, Kammermeier T, Dannhardt G, Kiefer W. Synthesis and evaluation of a novel series of pyrrolizine derivatives as dual cyclooxygenase-1 and 5-lipoxygenase inhibitors. *Arch Pharm Pharm Med Chem.* 1997;330:307–312. https://doi.org/10.1002/ardp.19973300908.
31. Abbas SE, Awadallah FM, Ibrahim NA, Gouda AM. Novel substituted and fused pyrrolizine derivatives: Synthesis, anti-inflammatory and ulcerogenecity studies. *Eur J Med Chem.* 2010;45:482–491. https://doi.org/10.1016/j.ejmech.2009.10.031.
32. Gouda AM, Ali HI, Almalki WH, Azim MA, Abourehab MAS, Abdelazeem AH. Design, synthesis, and biological evaluation of some novel pyrrolizine derivatives as COX inhibitors with anti-inflammatory/analgesic activities and low ulcerogenic liability *Molecules* 2016;21:201. https://doi.org/10.3390/molecules21020201.
33. Dannhardt G, Kiefer W, Nowe U. *E*-2-Pyrrolizin-5-yl acrylic acids as potent dual or selective inhibitors of bovine cyclooxygenase and 5-lipoxygenase. *Arch Pharm.* 1995;328:681–686. https://doi.org/10.1002/ardp.19953280910.
34. Barsoum FF. Synthesis and molecular modeling studies of anti-inflammatory active 1*H*-pyrrolizine-5-carboxamides. *Arch Pharm Chem Life Sci.* 2011;1:56–65. https://doi.org/10.1002/ardp.201000166.
35. Battilocchio C, Poce G, Alfonso S, Porretta GC, Consalvi S, Sautebin L, Pace S, Rossi A, Ghelardini C, Mannelli LDC, Schenone S, Giordani A, Di Francesco L, Patrignani P, Biava M. A class of pyrrole derivatives endowed with analgesic/anti-inflammatory activity. *Bioorg Med Chem.* 2013;21:3695–3701. https://doi.org/10.1016/j.bmc.2013.04.031.
36. Wiegard A, Hanekamp W, Griessbach K, Fabian J, Lehr M. Pyrrole alkanoic acid derivatives as nuisance inhibitors of microsomal prostaglandin E2 synthase-1. *Eur J Med Chem.* 2012;48:153–163. https://doi.org/10.1016/j.ejmech.2011.12.009.
37. Wilkerson WW, Galbraith W, Gans-Brags K, Grubbs M, Hewes WE, Jaffee B, Kenney JP, Kerr J, Wong N. Antiinflammatory 4,5-diarylpyrroles: Synthesis and QSAR. *J Med Chem.* 1994;37:988–998. https://pubs.acs.org/doi/pdf/10.1021/jm00033a017.
38. Biava M, Porretta GC, Poce G, Supino S, Forli S, Rovini M, Cappelli A, Manetti F, Botta M, Sautebin L, Rossi A, Pergola C, Ghelardini C, Vivoli E, Makovec F, Anzellotti P, Patrignani P, Anzini M. Cyclooxygenase-2 inhibitors. 1,5-Diarylpyrrol-3-acetic esters with enhanced inhibitory activity toward cyclooxygenase-2 and improved cyclooxygenase-2/cyclooxygenase-1 selectivity. *J Med Chem.* 2007;50:5403–5411. https://pubs.acs.org/doi/full/10.1021/jm0707525

39. Maddila S, Gorle S, Sampath Ch, Lavanya P. Synthesis and anti-flammatory activity of some new 1,3,4-thiadiazoles containing pyrazole and pyrrole nucleus. *J Saudi Chem Soc.* 2016;20:S306–S312. https://doi.org/10.1016/j.jscs.2012.11.007.

40. Sarg MT, Koraa MM, Bayoumi AH, Abd El Gilil, SM. Synthesis of pyrroles and condensed pyrroles as anti-inflammatory agents with multiple activities and their molecular docking study. *Open J Med Chem.* 2015;5:49–96. http://dx.doi.org/10.4236/ojmc.2015.54005.

41. Mohamed MS, Kamel R, Fathallah SS. Synthesis of new pyrroles of potential anti-inflammatory activity. *Arch Pharm Chem Life Sci.* 2011;344:830–839. https://doi.org/10.1002/ardp.201100056.

42. De Young LM, Kheifets JB, Ballaron SJ, Young JM. Edema and cell infiltration in the phorbol ester-treated mouse ear are temporally separate and can be differentially modulated by pharmacologic agents. *Agents Actions* 1989;26:335–341. https://doi.org/10.1007/BF01967298.

43. Bralley EE, Greenspan P, Hargrove JL, Wicker L, Hartle DK. Topical anti-inflammatory activity of *Polygonum cuspidatum* extract in the TPA model of mouse ear inflammation. *J Inflamm.* 2008;5:1. https://doi.org/10.1186/1476-9255-5-1.

44. Puigneró V, Turull A, Queralt J. Arachidonic acid (AA) and tetradecanoylphorbol acetate (TPA) exert systemic effects when applied topically in the mouse. *Inflammation.* 1998;22:307–314. https://doi.org/10.1023/A:1022352200273.

45. Patel M, Murugananthan, Gowda KPS. *In vivo* animal models in preclinical evaluation of anti-inflammatory activity– a review. *Int J Pharmacol Res Allied Sci.* 2012;1:1–5. http://www.ijpras.com.

46. Carson JR, Wong S. 5-Benzoyl-1-methylpyrrole-2-acetic acids as antiinflammatory agents. 2. The 4-methyl compounds. *J Med Chem.* 1973;16:172–174. https://pubs.acs.org/doi/pdf/10.1021/jm00260a023.

47. Martínez-Mora EI, Caracas MA, Escalante CH, Madrigal DA, Quiroz-Florentino H, Delgado F, Tamariz J. Divergent and selective functionalization of 2-formylpyrrole and its application in the total synthesis of the aglycone alkaloid pyrrolemarumine. *J Mex Chem Soc.* 2016;60:23–33. http://www.scielo.org.mx/pdf/jmcs/v60n1/1870-249X-jmcs-60-01-00023.pdf.

48. Martínez-Mora EI, Caracas MA, Escalante CH, Espinoza-Hicks C, Quiroz-Florentino H, Delgado F, Tamariz J. 2-Formylpyrroles as building blocks in a divergent synthesis of pyrrolizines. *Synthesis.* 2016;48:1055–1068. https://doi.org/10.1055/s-0035-1561331.

49. Campbell SE, Comer MC, Derbyshire PA, Despinoy XLM, McNab H, Morrison R, Sommerville CC, Thornley C. Synthesis of pyrrolizin-3-ones by flash vacuum pyrolysis of

pyrrol-2-ylmethylidene Meldrum's acid derivatives and 3-(pyrrol-2-yl)propenoic esters. *J Chem Soc Perkin Trans 1.* 1997;2195–2202. https://pubs.rsc.org/en/content/articlelanding/1997/p1/a701749i#!divAbstract

50. Mase N, Horibe T. Organocatalytic Knoevenagel condensations by means of carbamic acid ammonium salts. *Org Lett.* 2013;15:1854–1857. https://pubs.acs.org/doi/10.1021/ol400462d
51. Buchanan MS, Carroll AR, Addepalli R, Avery VM, Hooper JNA, Quinn RJ. Natural products, stylissadines A and B, specific antagonists of the $P2X_7$ receptor, an important inflammatory target. *J Org Chem.* 2007;72:2309–2317. https://pubs.acs.org/doi/abs/10.1021/jo062007q
52. Rane RA, Nandave M, Nayak S, Naik A, Shah D, Alwan WS, Sahu NU, Naphade SS, Palkar MB, Karunanidhi S, Thapliyal N, Karpoormath R. Synthesis and pharmacological evaluation of marine bromopyrrole alkaloid-based hybrids with anti-inflammatory activity. *Arabian J Chem.* 2017;10:458–464. https://doi.org/10.1016/j.arabjc.2014.06.004
53. Kida T, Kozai S, Takahashi H, Isaka M, Tokushige H, Sakamoto T. Pharmaokinetics and efficacy of topically applied nonsteroidal anti-inflammatory dfrugs in retinochoroidal tissues in rabbits. *Plos One.* 2014;9:e96481. http://doi:10.1371/journal.pone.0096481.
54. Unaleroglu C, Yazici A. Gadolinium triflate catalyzed alkylation of pyrroles: efficient synthesis of 3-oxo-2,3-dihydro-1*H*-pyrrolizine derivatives. *Tetrahedron.* 2007;63:5608–5613. https://doi.org/10.1016/j.tet.2007.04.018
55. Although in the original reference [54] no details were given about the diastereisomeric ratio for the annulation products, in a more recent work similar products were obtained as a mixture of diastereoisomers: Unaleroglu C, Tasgin DI, Aytac S, Temelli B. An efficient synthetic route for pyrrolizinone synthesis through functionalized *C*-alkylpyrroles. *Synthesis.* 2009;3243–3250. https://doi.org/10.1055/s-0029-1216951
56. Rodríguez-Díaz M, Delporte C, Cartagena C, Cassels BK, González P, Silva X, León F, Wessjohann LA. 2011. Topical anti-inflammatory activity of quillaic acid from *Quillaja saponaria* Mol. and some derivatives. *J Pharm Pharmacol.* 2011;63:718–724. https://doi.org/10.1111/j.2042-7158.2011.01263.x
57. Lemus-Mondaca R, Vega-Gálvez A, Rojas P, Stucken K, Delporte C, Valenzuela-Barra G, Jagus RJ, Agüero MV, Pasten A. Antioxidant, antimicrobial and anti-inflammatory potential of *Stevia rebaudiana* leaves: effect of different drying methods. *J Appl Res Med Aromat Plants*. 2018;11:37–46.
58. Gutiérrez-Rebolledo GA, Garduño-Siciliano L, García-Rodríguez RV, Pérez-González MZ, Chávez MI, Bah M, Siordia-Reyes GA, Chamorro-Cevallos GA, Jiménez-Arellanes MA.

Anti-inflammatory and toxicological evaluation of *Moussonia deppeana* (Schldl. & Cham) Hanst and Verbascoside as a main active metabolite. *J Ethnopharmacol.* 2016;187:269–280. https://doi.org/10.1016/j.jep.2016.04.033.

59. Morris GM, Huey R, Lindstrom W, Sanner MF, Belew RK, Goodsell DS, Olson AJ. AutoDock4 and AutoDockTools4: Automated docking with selective receptor flexiblity. *J Comput Chem.* 2009;30:2785–2791. https://doi.org/10.1002/jcc.21256
60. Furnham N, Laskowski RA, Thornton JM. Abstracting knowledge from the protein data bank. Biopolymers. 2013;99:183–188. https://doi.org/10.1002/bip.22107
61. Abdelgawad MA, Bakr RB, Azouz AA. Novel pyrimidine-pyridine hybrids: Synthesis, cyclooxygenase inhibition, anti-inflammatory activity and ulcerogenic liability. *Bioorg Chem.* 2018;77:339–348. https://doi.org/10.1016/j.bioorg.2018.01.028
62. Amin NH, El-Saadi MT, Hefny AA, Abdelazeem AH, Elshemy HAH, Abdellatif KRA. Anti-inflammatory indomethacin analogs endowed with preferential COX-2 inhibitory activity. *Future Med Chem.* 2018;10:2521–2535. https://doi.org/10.4155/fmc-2018-0224
63. Sakr A, Kothayer H, Ibrahim SM, Baraka MM, Rezq S. 1,4-Dihydroquinazolin-3(2H)-yl benzamide derivatives as anti-inflammatory and analgesic agents with an improved gastric profile: Design, synthesis, COX-1/2 inhibitory activity and molecular docking study. *Bioorg Chem.* 2019;84:76–86. https://doi.org/10.1016/j.bioorg.2018.11.030
64. Mosmann T. Rapid colorimetric assay for cellular growth and survival: Application to proliferation and cytotoxicity assays. *J. Immunol Methods*. 1983;65:55–63. https://doi.org/10.1016/0022-1759(83)90303-4
65. Williams CS, Watson AJM, Sheng H, Helou R, Shao J, DuBois RN. Celecoxib prevents tumor growth *in vivo* without toxicity to normal gut: Lack of correlation between *in vitro* and *in vivo* models. *Cancer Res.* 2000;60:6045–6051.
66. Kanno S, Shouji A, Tomizawa A, Hiura T, Osanai Y, Ujibe M, Obara Y, Nakahata, N, Ishikawa M. Inhibitory effect of naringin on lipopolysaccharide (LPS)-induced endotoxin shock in mice and nitric oxide production in RAW 264.7 macrophages. *Life Sci.* 2006;78:673–681. https://doi.org/10.1016/j.lfs.2005.04.051
67. Posadas I, Terencio MC, Guillén I, Ferrándiz ML, Coloma J, Payá M, Alcaraz MJ. Co-regulation between cyclo-oxygenase-2 and inducible nitric oxide synthase expression in the time-course of murine inflammation. *Naunyn-Schmiedeberg's Arch. Pharmacol.* 2000;361:98–106. https://doi.org/10.1007/s002109900150
68. Lee JK. Anti-inflammatory effects of eriodictyol in lipopolysaccharide-stimulated raw 264.7 murine macrophages. *Arch. Pharm. Res.* 2011;34:671–679.

https://doi.org/10.1007/s12272-011-0418-3

69. Ahn KS, Noh EJ, Zhao HL, Jung SH, Kang SS, Kim YS. Inhibition of inducible nitric oxide synthase and cyclooxygenase II by *Platycodon grandiflorum* saponins via suppression of nuclear factor-κB activation in RAW 264.7 cells. *Life Sci.* 2005;76:2315–2328. https://doi.org/10.1016/j.lfs.2004.10.042

70. Koriatopoulou K, Karousis N, Varvounis G. Novel synthesis of the pyrrolo[2,1-c][1,4]benzodiazocine ring system via a Dieckmann condensation. *Tetrahedron.* 2008;64:10009–10013. https://doi.org/10.1016/j.tet.2008.07.029

71. Ogiwara Y, Takahashi K, Kitazawa T, Sakai N. Indium(III)-catalyzed Knoevenagel condensation of aldehydes and activated methylenes using acetic anhydride as a promoter. *J Org Chem.* 2015;80:3101–3110. https://pubs.acs.org/doi/10.1021/acs.joc.5b00011

72. McHugh M. L. Multiple comparison analysis testing in ANOVA. *Biochemia Med.* 2011;21:203–209. https://www.biochemia-medica.com/en/journal/21/3/10.11613/BM.2011.029

73. One-way ANOVA with Student Newman Keuls Test was performed using GraphPad Prism versión 5.00 for Windows, GraphPad Software, La Jolla California USA, http://www.graphpad.com.

74. Irwin JJ, Shoichet BK. ZINC – A free database of commercially available compounds for virtual screening. *J Chem Inf Model.* 2005;45:177–182. https://pubs.acs.org/doi/abs/10.1021/ci049714%2B

75. Frisch MJ, Trucks GW, Schlegel HB, Scuseria GE, Robb MA, Cheeseman JR, et al. Gaussian 98 Inc., Version A.6, Wallingford CT, 2004. http://gaussian.com/g03citation/ http://gaussian.com/

76. Dassault Systèmes BIOVIA, Discovery Studio Modeling Environment; Release 2017; Dassault Systèmes, San Diego: CA, 2016. https://www.3dsbiovia.com/products/collaborative-science/biovia-discovery-studio/

77. Kang Y-J, Wingerd BA, Arakawa T, Smith WL. Cyclooxygenase-2 Gene Transcription in a Macrophage Model of Inflammation. J. Immunol. 2006;177:8111–8122. https://doi.org/10.4049/jimmunol.177.11.8111

GRAPHICAL ABSTRACT

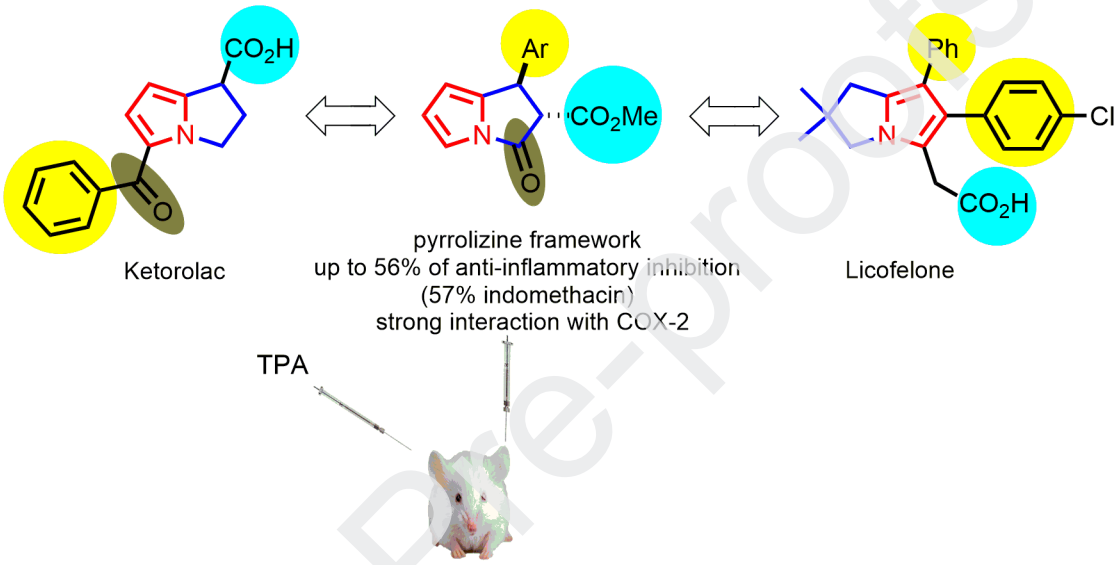

Synthesis and highly potent anti-inflammatory activity of licofelone- and ketorolac-based 1-arylpyrrolizin-3-ones

Damian A. Madrigal,[a,b,†] Carlos H. Escalante,[a,†] Gabriel A. Gutiérrez-Rebolledo,[b] José M. Cristobal-Luna,[b] Omar Gómez-García,[a] Roberto I. Hernández-Benitez,[a] Ana L. Esquivel-Campos,[c] Salud Pérez-Gutiérrez,[c] Germán A. Chamorro-Cevallos,[b,*] Francisco Delgado[a] and Joaquín Tamariz[a,*]

Conflict of interest

The authors declare that they have no conflict of interest.

GRAPHICAL ABSTRACT